Three dimensional spheroid cell culture of human MSC-derived neuron-like cells: new in vitro model to assess magnetite nanoparticle-induced neurotoxicity effects

Journal:	*Journal of Applied Toxicology*
Manuscript ID	JAT-21-0565.R2
Wiley - Manuscript type:	Research Article
Date Submitted by the Author:	19-Jan-2022
Complete List of Authors:	De Simone, Uliana; Maugeri Clinical Research Institutes IRCCS, Croce, Anna ; National Research Council Pignatti, Patrizia; Maugeri Clinical Research Institutes IRCCS Buscaglia, Eleonora; Maugeri Clinical Research Institutes IRCCS, Caloni, Francesca; Università degli Studi di Milano Coccini, Teresa; Maugeri Clinical Research Institutes IRCCS
Keywords:	in vitro alternative methods, predictive nanotoxicology, mesenchymal stem cells, occupational and environmental health, risk assessment

Three dimensional spheroid cell culture of human MSC-derived neuron-like cells: new in vitro model to assess magnetite nanoparticle-induced neurotoxicity effects.

Running Head: 3D human neuron-like cells as new model for neurotoxicity testing

Uliana De Simone[1], Anna Cleta Croce[2], Patrizia Pignatti[3], Eleonora Buscaglia[1], Francesca Caloni[4], Teresa Coccini[1*]

[1] Laboratory of Clinical and Experimental Toxicology, and Pavia Poison Centre - National Toxicology Information Centre, Toxicology Unit, Istituti Clinici Scientifici Maugeri IRCCS, Pavia, Italy.

[2] Institute of Molecular Genetics, Italian National Research Council (CNR), Pavia, Italy, and Department of Biology & Biotechnology, University of Pavia, Pavia, Italy.

[3] Allergy and Immunology Unit, Istituti Clinici Scientifici Maugeri IRCCS, Pavia, Italy.

[4] Department of Health, Animal Science and Food Safety, Universitá degli Studi di Milano, Milan, Italy.

*** Correspondence to:**

Teresa Coccini
Istituti Clinici Scientifici Maugeri IRCCS
Via Maugeri 4, 27100 Pavia, Italy.
phone: +39-0382-592416
email: teresa.coccini@icsmaugeri.it

Abstract

As nanoparticles (NPs) can access the brain and impact on CNS function, novel *in vitro* models for the evaluation of NPs-induced neurotoxicity are advocated. 3D-spheroids of primary neuron-like cells (hNLCs) of human origin have been generated, from differentiation of human umbilical cord mesenchymal stem cells (MSCs). The study evaluated Fe_3O_4NP impact on the differentiation process by applying the challenge at complete 3D hNLC spheroid formation (after 4 days-T4) or at beginning of neurogenic induction/simultaneously 3D forming (T0). Different endpoints were monitored over time (up to 10 days): spheroid growth, size, morphology, ATP, cell death, neuronal markers (β-Tub III, MAP-2, NSE), NP-uptake.

At T0-application, a marked concentration- and time-dependent cell mortality occurred: effect started early (day 2) and low concentration (1 µg/ml) and exacerbated (80% mortality) after prolonged time (day 6) and increased concentrations (50 µg/ml). ATP was strikingly affected. All neuronal markers were downregulated and spheroid morphology altered in a concentration-dependent manner (from ≥ 5µg/ml) after day 2.

Fe_3O_4NPs applied at complete 3D formation (T4) still induced adverse effects although less severe: cell mortality (20-60%) and ATP content decrease (10-40%) were observed in a concentration-dependent manner (from ≥ 5 µg/ml). A neuronal-specific marker effect and spheroid size reduction from 25 µg/ml without morphology alteration were evidenced.

This finding provides additional information on neurotoxic effects of Fe_3O_4NPs in a new 3D hNLC spheroid model derived from MSCs, that could find a consistent application as in a testing strategy serving in first step hazard identification for correct risk assessment.

Short Abstract

Human 3D-spheroids of neuron-like cells (hNLC) were generated from differentiation of umbilical cord mesenchymal stem cells.

When Fe_3O_4NPs were applied at beginning of neurogenic induction/simultaneously 3D forming, marked toxicity occurred early (day2) and from 5µg/ml. Fe_3O_4NPs applied at complete 3D formation still induced adverse effects although less severe. This finding provides additional information on neurotoxic effects of Fe_3O_4NPs in a new 3D-hNLC spheroid model, that could find a consistent application as in a testing strategy serving in first step hazard.

Keywords:

in vitro alternative methods; predictive nanotoxicology; mesenchymal stem cells; occupational and environmental health; risk assessment

1. Introduction

With the development of nanotechnologies, even if towards a safe and sustainable innovation (Gottardo et al., 2021), uncertainties associated with the health and environmental impacts of free and manufactured nanoparticles (NPs) are growing.

Regardless of the exposure route, once NPs are in the body they are distributed by the bloodstream and translocated to the brain (Cupaioli et al., 2014; Hu & Gao, 2010). A serious damage, as a consequence of direct exposure to NPs in utero, is reported (Bongaerts et al., 2020; Win-Shwe & Fujimaki, 2011) and NP distribution raises a particular concern when transferred from placenta to the fetal central nervous system (CNS) (Willmann & Dringen, 2019). All these aspects explain the great attention and increasing interest on the neurotoxic effects of the NPs (Chang et al., 2021; Wang et al., 2017; Win-Shwe & Fujimaki, 2011; Wu & Tang, 2018).

Even if the procedures for the evaluation of NP toxicity have not yet been defined, the *in vitro* approach is promising in testing strategy for risk assessment (Sambuy et al., 2018). Cell-based models of human origin are strongly recommended as more appropriate alternative methods in species-specific extrapolation of results to improve prediction and mechanistic knowledge in toxicology (Bal-Price et al., 2018; NRC, 2007; Tukker et al., 2016). In this context, the *in vitro* human stem cells (hSCs) models currently represent one of the innovative technologies for developing assays and tools (Kim et al., 2019; Knudsen et al., 2015). Along these lines, SC-derived *in vitro* tools may provide more realistic platforms for nanotoxicology study (Handral et al., 2016; Stueckle & Roberts, 2019; Suma & Mohanan, 2015). hSCs have, as advantage over primary and immortalized cells, the remarkable ability for self-renewal, long-term proliferation, and plasticity potential towards the development of variety of cell types including neuronal and glial cells (Singh & Kashyap, 2016).

Among the different stem cells categories, depending upon the source of origin, the human umbilical cord-derived mesenchymal stem cells (MSCs) have the advantages of simple convenient preparation, feasible source, more primitive properties (i.e., fetal in nature), higher proliferation capacity. Moreover, a recent study analysed large sample size of MSCs from umbilical cord revealing a consistency between donors (Raileanu et al., 2019). These properties make MSCs valuable tools to be used for *in vitro* toxicology investigations as well as developmental neurotoxicity studies. Furthermore, these stem cells are advantageous because they do not form tumors (Singh et al., 2015). Recent advances have demonstrated that cells of nonmesodermal origin including neuron-like cells (hNLCs) can be efficiently obtained from the *in vitro* transdifferentiation of the MSCs derived from human umbilical cord (Cortés-Medina et al., 2019; Czarnecka et al., 2017; Hernández et al., 2020; Kil et al., 2016; Shahbazi et al., 2016; Shi et al., 2018; Singh & Kashyap, 2016). The plasticity of the hMSCs related to their differentiation into proper neuronal lineages is an increasingly valued tool for the development of alternative cell therapies for the treatment of the nervous system disorders (Hernández et al., 2020), but also can represent a promising source of cells for the screening evaluation of potential neuronal toxicity of NPs in humans (Kim et al., 2019; Suma &Mohanan, 2015).

In this respect, a recent developed *in vitro* model of hNLCs generated from MSCs derived from human umbilical cord lining membranes (Coccini et al., 2020; De Simone et al., 2020), combined with a test battery, can be a useful tool in risk assessment for emerging contaminants, and the three-dimensional shape (3D), if compared with the widely used two-dimensional (2D) cell culture (Petros & DeSimone, 2010), mimicking better the *in vivo* situation, seems to be more effective (Langhans, 2018) and, multicellular spheroids found their application in many fields from oncology to tissue engineering (Cesarz & Tamama, 2016).

3D CNS cultures have demonstrated advantages compared to 2D cultures, such as increased cell survival and differentiation and better reproduction of electrical activity (Jurga et al., 2009; Pamies et al., 2014) compared to animal models, in terms of human relevance (Gibb, 2008; Lee & Lee, 2020), as evidenced by increase of studies using a variety of such models to evaluate nanotoxicity

and NP neurotoxicity (De Simone et al., 2018; Goodman et al., 2008; Hoelting et al., 2013; Joshi et al., 2020; Kobolak et al., 2020; Lee et al., 2009; Leite et al., 2019; Sreekanthreddy et al., 2015; Zeng et al., 2016).

Among the engineered nanoparticles, metal NPs and metal oxide NPs account for the largest share in terms of manufacture and application (Djurisic et al., 2015; Wu & Tang, 2018) and some of these NPs exist in the environment as components of dust and smoke (Bai & Tang, 2020). Even if neurotoxicological effects were demonstrated with metal-containing NPs (Chang et al., 2021), their application in medicine is widespread, as it results for iron oxide nanoparticle (IONPs), like magnetite (Fe_3O_4NPs) (Akbarzadeh et al., 2012). The IONPs are highly versatile and are applied in many domains, but are able to reach the brain, exerting possible adverse effects (Landrigan & Miodovnik, 2011; Maher et al., 2016, 2019; Shi et al., 2016; Sly & Flack, 2008; Willmann & Dringen, 2019).

In this study we firstly developed, optimized and characterized a new human 3D neuronal *in vitro* model using primary neuron-like cells (hNLCs) generated from the MSCs derived from human umbilical cord lining membranes (hMSCs) using ULA 96-well round-bottomed plates. The investigation aimed at evaluating the impact of Fe_3O_4NP exposure on 3D neuron-like differentiation process from hMSCs, by applying the challenge (a single treatment) at the beginning of the transdifferentiation process (neurogenic induction) and simultaneously 3D forming (namely T0) as well as the effects after short-term (24 and 48 h) exposure challenged at complete neuron 3D formation (namely after 4 days - T4). In the latter, the cells were allowed to form spheroids (equilibration) prior NP exposure, while in the former model, the cells were treated with NPs directly during process of the spheroid formation. The rationale of the exposure of spheroids before and after neuronal differentiation is related to the final different reaching endpoints. The spheroid exposure at the beginning of differentiation permits to evaluate the effects of NPs during the different early stages of the neurodevelopment, while the exposure after neuronal differentiation take into account the effects on established spheroids.
Different endpoint parameters such as ATP, cell death (by Trypan blue), neuronal markers expressions (β-Tubulin III, MAP-2, enolase, and Nestin), and intracellular uptake of NPs during hNLCs differentiation/3D spheroid formation have been assessed for identifying the adverse effects and molecular mechanisms induced by NPs exposure on nervous system. hNLC spheroid growth, size and morphological changes were analysed by light microscopy. Analysis of the internal spheroid structure evidenced by Hematoxylin and Eosin (H&E) staining was also monitored during time. Fe_3O_4NP uptake into spheroids was detected by Perls' Prussian blue staining.

2. Materials and Methods

2.1. Chemicals and Reagents

Mesenchymal stem cell growth medium 2 (Ready-to-use) (PromoCell), mesenchymal stem cell neurogenic differentiation medium (Ready-to-use) (PromoCell), human fibronectin solution (1 mg/ml) (PromoCell), and all cell culture reagents were purchased from Carlo Erba Reagents s.r.l (Cornaredo, Italy). Tissue culture flasks (75 cm^2; Corning), ULA 96-well round-bottomed plates ultra-low attachment (Corning) and 0.4% Trypan Blue solution (Corning) were purchased from VWR (Italy). Accutase (DUTSCHER) was purchased from BioSigma (Cona, Italy). CellTiter-Glo® 3D Cell Viability assay was acquired from Promega (Milan, Italy). Primary antibodies conjugated to alexa-fluo®488 or 594 were obtained from D.B.A. Italia s.r.l (Segrate, Italy) for enolase (NSE) (Santa Cruz Biotechnology) and Merck (Milan, Italy) for β-Tubulin III (β-Tub III) (Merck), Microtubule-associated protein 2 (MAP-2) (Merck) and Nestin (Merck). BD cytofix/cytoperm kit was acquired from BD Biosciences (Milan, Italy). Polyvinylpyrrolidone coated Fe_3O_4NPs were

obtained from nanoComposix (San Diego, CA, USA; lot no. ECP1475). Silane-prep slide glasses, Neo-Mount and Fluoroshield were purchased from Merck (Milan, Italy). Hoechst 33258 (Invitrogen) was purchased by Life Technologies Italia (Monza, Italy).

2.2. Human neuronal spheroids formation and growth from primary neuron-like cells (hNLCs) derived from human umbilical cord lining membranes

The neuronal spheroids were obtained starting from primary neuron-like cells (hNLCs) derived from the transdifferentiation of the human mesenchymal cells isolated from human umbilical cord lining membranes (hMSCs). Umbilical cords were collected from full-term pregnant women during elective cesarean sections as described in (Coccini et al., 2019) and hMSCs were routinely cultured in 75 cm^2 flasks using mesenchymal stem cell growth medium 2 and maintained at 37 °C in a humidified atmosphere of 95% air/5 % CO_2.

hMSCs were seeded at different cell density specifically: 10000, 25000, 50000 and 100000 cells per well in 200 µl of mesenchymal stem cell neurogenic differentiation medium in ULA Plates coated with human fibronectin (10 µg/ml). This point refers to time 0 (T0). Old medium was carefully changed with fresh medium every 48 h: 100 µl was removed and replenished with another 100 µl of fresh medium.
Morphology and growth of the spheroids were monitored over time (at day 2, 4, 6, 10) using an inverted phase-contrast microscope (Zeiss Axiovert 25 microscope) equipped with a 10X objective. Spheroid area was also analysed via light microscopy utilising a phase-contract microscope (Zeiss Axiovert 25 microscope). Images were taken at 10X magnification using a digital camera (Canon powershot G8) and processed using Image J software 1.51 (NIH, Massachusetts, USA) to evaluate the size of the spheroids, and an objective calibration slide was used to calculate the spheroid area. The colour captured images (n=8), derived from each condition, were converted to binary images and analysed with the ‘‘Measure tool”. Data analysis was performed in Microsoft Excel. We assumed that all spheroids have a round shape, and therefore the diameter of the spheroids was determined from their area.

2.3. Physico-chemical properties of Fe_3O_4NP Stock Suspension

The physico-chemical properties of Fe_3O_4NP stock suspension in a 2 mM citrate solution were provided by the manufacturer (nanoComposix Company). The particles appear dark brown in colour, showed a roughly spherical shape almost non-agglomerated (Ø: 20.3 ± 5 nm, by TEM) with a hydrodynamic diameter of 42 nm, surface area of 50.2 m^2/g (by TEM), mass concentration of 20.3 mg/ml, zeta potential of - 51 mV, and pH solution 7.4. Physico-chemical Fe_3O_4NPs properties in mesenchymal stem cell neurogenic differentiation medium were performed using the Malvern Zetasizer Nano ZS90 (N.A.M. S.r.l., NANO-Analysis and Materials, Gazzada Schianno, Varese, Italy) as described in De Simone et al. (2020).

2.4. Nanoparticles testing (Fe_3O_4NP exposure)

Two different exposure approaches were applied (see scheme in Fig. 1). In the first approach, the hNLC spheroids were treated with Fe_3O_4NPs at day 4 (T4) of the neurogenic induction when the spheroids were well formed and tight aggregated.
Treatment suspensions were prepared by dissolving Fe_3O_4NPs stock suspension in mesenchymal stem cell neurogenic differentiation medium and vortexed immediately before each use. hNLC spheroids were exposed for 24 (T5) and 48 h (T6) to increasing concentrations of Fe_3O_4NPs (5-100 µg/ml) and potential Fe_3O_4NP-induced toxicity effects were evaluated.
In the second approach, hNLCs were treated with Fe_3O_4NPs (1-50 µg/ml) at time T0 of both spheroid formation and neurogenic differentiation process in 96-ULA plate. Old medium was carefully changed with fresh medium every 48 h. The microtissue formation in the presence of nanoparticles and the toxicological evaluation were performed at day 2, 3, 4, 5 and 6.

In both exposure approaches, the T0 seeded spheroids were 25000 cells/well in 200 µl mesenchymal stem cell neurogenic differentiation. This setting was chosen based on the optimal density condition obtained for this cell number resulting from the linearity study as indicated in the previous paragraph.
Multiple endpoints of toxicity in terms of morphological changes of shape (by light microscopy and H&E staining), expression of neuronal markers (by immunofluorescence and flowcytometry), cell viability (by Trypan blue exclusion test) and ATP content were evaluated. The uptake of Fe_3O_4NPs was also detected by Perls' Prussian blue staining.
After both types of NP treatments (i.e., T4 and T0), before performing each different test, the treated spheroids were washed with PBS to remove any residue of Fe_3O_4NPs in the medium suspension.

2.5. Morphological analysis by light phase-contrast microscopy
The hNLC spheroids were observed under an inverted phase-contrast microscopy equipped with a 10X objective, after Fe_3O_4NP exposure in order to analyze the healthy status of the cells, the spheroid growth/size and the morphological changes induced by Fe_3O_4NP treatments. Digital photographs were captured with a camera (Canon powershot G8) and stored on the PC. The area of spheroid was calculated as described in "Human neuronal spheroids formation".

2.6. Frozen sections of hNLC spheroids for immunofluorescence and histochemistry analysis
After each exposure time point, the culture medium was carefully removed from each well and at least 16-24 spheroids per condition were pooled, washed with phosphate-buffered saline (1 ml/tube PBS), fixed in 4% paraformaldehyde solution (PF; for 60 min at room temperature (r. t.)), washed again. Then spheroids were cryoprotected. Specifically: the spheroids were submerged in 10% sucrose in PBS solution (500 µl/tube; for 30 min r.t.), then centrifuged, re-submerged in 20% sucrose in PBS solution (500 µl/tube; for 30 min r.t.), finally, in 30% sucrose in PBS solution (500 µl/tube) overnight at +4 °C. The next day, after removing 30% sucrose in PBS solution, the spheroids were embedded in optimal cutting temperature compound (OCT) and stored at -80 °C until use. Ten-µm thick cryostatic sections were cut by using a cryostat (Leica CM 1850, Leica Microsystems, GmbH, Wetlzar, Germany), and deposed on silane prep slides for next staining and labelling processes. Representative sections (from each concentration and for each time point) were obtained from n=10-15 sequential sections.

2.6.1. Fe_3O_4NPs uptake and Haematoxylin & Eosin (H&E) staining
Perls' Prussian blue staining has been used to evaluate the uptake of Fe_3O_4NPs. The method has been adopted from Rowatt et al. (2018). Briefly, frozen sections of hNLCs placed on glass slides coated with silane were thawed, dried at r.t. and rehydrated in distilled water for 10 min. Then the cryo-sections were covered with Perls' solution (1:1 solution 2% of $K_4[Fe(CN)_6]$ and solution 6% HCl; 2 ml/well) for 30 min at r.t. and rinsed with distilled water (2 min). Afterward, the cryo-sections were stained with Shandon Instant Haematoxylin (15 min at r.t.), rinsed with tap water (20 s), dipped in differentiate solution (1% HCl in 70% ethyl alcohol), again rinsed with tap water, then the nuclei were stained with 1% ammonium hydroxide solution (10 s at r.t.), washed and rinsed in 95% alcohol solution (5 min r.t.). After all, the cryo-sections were covered with 1% alcoholic eosin Y (1 min at r.t.) and dehydrated in increasing alcohol gradient and finally mounted with Neo-Mount. The images were acquired using a light microscopy (Zeiss AXIOSKOP 40/40FL microscope) equipped with objective (20X) lens, and a digital camera (AxioCam MRc5 Zeiss).

2.6.2. Neuronal markers expression

2.6.2.1. Immunofluorescence analysis

After rehydration, the cryo-sections of the spheroids were permeabilized (with 0.25% Triton X-100 in PBS solution for 10 min at r.t.) and incubated for 30 min in blocking buffer (1% BSA in PBS). Then they were incubated with primary antibodies alexa-fluo®488 or 594 conjugate against: β-Tub III (1:100), MAP-2 (1:100) and NSE (1:100) diluted in 1% bovine serum albumin (BSA) solution for 60 min r.t. in dark. After washing in PBS (three times; 5 min. for each washing) the nuclei were detected using Hoechst 33258 (5 μM) or propidium iodide (1 μg/ml) for 10 min at r.t., and finally the spheroid sections were mounted with Fluoroshield. Fluorescence images were acquired using a CX41 Olympus fluorescence microscope combined with digital camera and equipped with 20X objective, excitation light being provided by EPI LED Cassette and combined with digital camera. Measurement conditions were the following: 470 nm excitation (T%= 40), 505 nm dichroic beamsplitter, and 510 nm long pass filter.

2.7. Flow cytometry analysis

Single cells within spheroids were analyzed by flow cytometry. Briefly, spheroids (n=24 for each different conditions) were washed with PBS and dissociated in Accutase (100 μl/well, up to 30 min at r.t.). Afterwards, an equal volume of fetal bovine serum (FBS) 2% solution was added and cells were resuspended and counted using the Burker chamber to determine the cell viability by Trypan blue test. Subsequently, the cells were fixed, permeabilized and incubated with primary antibodies alexa-fluo®488 or 594 conjugate against: β-Tub III (1:10000), MAP-2 (1:200), NSE (1:50), and Nestin (1:500), using the BD cytofix/cytoperm kit according to the manufacturer's instructions. Samples were acquired with a two laser flow cytometer (FACSCantoII) and analyzed with Diva Software (BD Biosciences). Values are expressed as MFI (median fluorescent intensity).

2.8. Trypan Blue test (TB)

Trypan Blue exclusion test is based on the principle that live cells prevent the dye penetration, such as trypan blue, since they possess the membrane integrity whereas dead cells do not. The cell suspension was mixed with trypan blue 0.4% solution then visually examined to determine whether cells take up or exclude dye.

At the end of the different treatment with Fe_3O_4NPs, the culture media were carefully aspirated, and the spheroids washed with PBS, dissociated with Accutase, and cells resuspended in neurogenic medium and counted using the Burker chamber in order to determine cell viability.

2.9. ATP evaluation by CellTiter-Glo® 3D Assay

The number of viable cells in 3D cell culture was determined using a luminescence-based test method namely "CellTiter-Glo® Luminescent Cell Viability Assay" whose principle is based on quantitation of the ATP (indicator of cell metabolism). The ready-to-use solution results in the cell lysis and generation of a luminescent signal which is directly proportional to the amount of ATP. The luminescence measurement was performed by a microplate fluorometer (Fluoroskan, Thermo Scientific, Milan, Italy). The blank reaction was used for the background luminescence associated with the specific medium used and reagent. Then, the experimental values were subtracted from the blank value.

2.10. Statistical analysis

Data of cell viability, ATP content, flow cytometric analysis, and size (diameter, area) evaluation are shown as mean ± S.E. of three separate experiments, each carried out in four or eight replicates. Statistical analysis was performed by One-way ANOVA, followed by Tukey's multiple comparisons test. *P* values less than 0.05 were considered to be significant.

3. Results

3.1. Physico-chemical properties of Fe_3O_4NPs

The Fe_3O_4NPs surface was provided coated with polyvinylpyrrolidone in order to give a steric stability. Physico-chemical properties of Fe_3O_4NPs in medium used for the transdifferentiation (as detailed in De Simone et al., 2020) are shown in Fig. 2. Neurogenic medium was renewed every 48 h and accordingly the parameter evaluation was performed up to 48 h. Fe_3O_4NPs exhibited fast agglomeration/aggregation when they were dispersed in the culture medium as shown by the hydrodynamic size measurements (size about 1200) after 30 min (De Simone et al., 2020). Aggregation still persisted after 24 and 48 h as indicated by a diameter of about 1300-1500 nm (Fig. 2).

3.2. Characterization of hNLC spheroids: neurogenic induction plus spheroid formation up to 10 days

3.2.1. Optimisation of spheroid starting cell number

Our first aim was to characterize the timewise differentiation of 3D neuronal spheroids free-floating in suspension culture, originating from hMSCs. For hNLC spheroid formation, the 96-ULA plates were used. Their characteristic design minimizes cell adherence to the bottom of the cell culture, but at the same time, increases interactions with neighbouring cells, and drives and positions a single spheroid within each well. Optimal conditions for hNLC spheroids have been evaluated. For that purpose, different cell numbers were seeded to generate hNLC spheroids of various size as shown in Fig. 3. Spheroids were formed from a starting cell number of 10000, 25000, 50000, 100000 mesenchymal stem cells and cultured in neurogenic medium for 10 days. Brightfield microscopy was used to measure spheroid area and morphology every two days (Fig. 3). Monitoring of hNLC spheroid formation and growth by microscopy showed that: when cells were seeded at the lowest concentration (i.e., 10000 cells/well), the cells formed loose cell aggregates, flat broad discs, and their shape did not change within 10 days of observation (Fig. 3) as also indicated by the area measurements. Cells did not form compact spheroids during the observation period (up to 10 days) (Fig. 3). These spheroids were less uniform and less stable in shape, resulting in disaggregation of some cells.

All the other starting cell numbers ($\geq$ 25000) resulted in the formation of spheroids of varying sizes, with all of the cells in each well aggregating to form a single spheroid. In particular, cells seeded at 25000 cells/well formed a spherical compact spheroid 2 days after seeding (Fig. 3) that became tight aggregate at day 4. The spheroids lost their compactness and began to disperse cells peripherally starting at day 6. In fact, spheroid area decrease was time-dependent. Notably, shape was quite homogeneous over time (up to 10 days) (Fig. 3). The two other cell plating densities tested, i.e. 50000 and 100000 cells/well, both produced compact hNLC spheroids whose compactness decreased over time in association with an increase cells detachment from the main body (dispersed peripherally), while, the shape resulted quite homogeneous over 10 days. Again, the spheroid area decreased in a time-dependent manner (Fig. 3).

Based on the above findings, the T0 seeded spheroids, for all further experiments, was set at 25000 cells/well. This setting was chosen based on the optimal density condition obtained for this cell number resulting from the above linearity study for creating spheroids that stayed the most uniform in shape over 10 days. The day 4 also appeared the ideal time to obtain optimal hNLC spheroids to be used for the Fe_3O_4NP treatment (first approach of exposure). Spheroids showed an area of 0.176 $\pm$ 0.002 mm^2 (diameter of 472 $\pm$ 2.5 µm).

3.2.2. Internal spheroid structure

The inner cell morphology and their arrangement were analyzed on spheroids with 25000 starting cell number from day 2 to day 10 after H&E staining (Fig. 4). A compact and uniform structure, and a well-defined external perimeter were observed in the stained sections of the spheroids. This kind of architecture and organization was similar for each condition up to 10 days (Fig. 4). hNLC

spheroids showed a well-defined circular structure and two morphologically different areas were identified, namely an outer layer composed of elongated cells and a central region consisting in layers of tightly packed predominately composed of triangular-shape cells with round nucleus. No necrotic core or hypoxia, in terms of reduced cell density and apoptotic nuclei, was present, as indicated by absence of pale eosinophilic cytoplasm in the core of spheroid sections (Fig. 4).

3.2.3. Neuronal markers (from day 1 to 10)

3.2.3.1. Immunofluorescence

The expression of β-Tub III (green fluorescence), MAP-2 (green fluorescence), and NSE (red fluorescence) in hNLC spheroids from day 2 to 10 was confirmed by immunofluorescence staining. The fluorescence intensity of β-Tub III (typically in soma and neurite-like processes), MAP-2 (typically evidenced into cytoplasm and neurite-like processes), and NSE (evidenced into cytoplasm) enhanced progressively over time in parallel with the transdifferentiation process of hNLC spheroids cultured in neurogenic medium (Fig. 5).

3.2.3.2. Flow cytometric analysis

Flow cytometric analysis also revealed that β-Tub III, MAP-2, and NSE started to be expressed early (day 1). MFI value of β-Tub III increased by 15%, MAP-2 by 30%, and NSE by 90% from day 1 to 10, as shown in Fig. 6. Differently, Nestin, a protein marker for neural stem cells, decreased over time indicating an early presence and later downregulation: MFI was high at the early time point (day 1) and decreased to about 60% with the neuronal differentiation (on day 10) (Fig. 6).

3.3. First treatment approach with Fe_3O_4NPs: treatment at day 4 (T4) and evaluation after 24 (T5) and 48 h (T6).

3.3.1. Cytotoxic effects

A concentration-dependent decrease (from 20 to 60 %) of viability evaluated by Trypan blue exclusion test was observed after 24 h exposure to Fe_3O_4NPs (from 5 to 100 μg/ml). Similar effects were detected after 48 h treatment (Fig. 7A).
A decrease of ATP content (from 10 to 40%) in a concentration-dependent manner was also detected after 24 h to Fe_3O_4NPs (from 5 to 100 μg/ml). Again, similar effects were detected after 48 h treatment (Fig. 7B).

3.3.2. Morphology analysis

Fe_3O_4NP treatments did not cause morphological alterations although NPs internalized in a concentration-dependent manner. Fe_3O_4NPs were also visible extra-spheroids (Fig. 8A). Notably, Fe_3O_4NPs induced a size reduction (about 10%) of spheroids starting from 25 μg/ml already after 24 h exposure and lasting even after 48 h (Fig. 8B).

3.3.3. Fe_3O_4NP uptake

Fe_3O_4NP uptake into hNLCs spheroids, evaluated by Perls' Prussian blue staining, was time- and concentration- dependent. Fe_3O_4NPs were immediately (24 h) evident in the outer layer of the spheroids starting from the lowest concentration tested (10 μg/ml). At the higher concentrations (25-50 μg/ml) the uptake steadily increased in the inner layers of the spheroids. After 48 h, NPs were also detected in the spheroid cores (Fig. 9).

3.3.4. Neuronal markers evaluation

Fe_3O_4NP treatments apparently affected some neuronal markers during transdifferentiation of hMSCs into hNLC spheroids as assessed by immunofluorescence microscopy. Decrease of the fluorescence intensity was observed after 24 h starting from 25 µg/ml for MAP-2 and NSE. These effects persisted up to 48 h. While β-Tub III was affected only after 48 h at 50 µg/ml (Fig. 10). Black spots of Fe_3O_4NPs were also visible inside hNLC spheroids after 24 and 48 h and were more evident when the concentrations increased.

Evaluation by flow cytometry indicated that Fe_3O_4NP exposure, from 10 to 50 µg/ml, starting at day 4 significantly downregulated the β-Tub III, MAP-2, NSE proteins differentiation in hNLC spheroids in a concentration- and time-dependent manner differently for each specific marker. The most affected marker was MAP-2 in that a significant effect was observed after 24 h (T5) (37-68% decrease) persisting after 48 h (T6) (20-47% decrease) and appearing at 10 µg/ml (Fig. 11). NSE was affected (12-28 % decrease) later (after 48 h exposure - T6) in a concentration-dependent manner. β-Tub III was affected (50% decrease) after 48 h (T6) at 50 µg/ml only (Fig. 11).

3.4. Second treatment approach with Fe_3O_4NPs: treatment at T0 of neurogenic induction and hNLC spheroid formation and evaluation at different time points

3.4.1. Cytotoxic effects

A marked concentration-dependent decrease of viability, evaluated by Trypan Blue (TB) test, was observed after Fe_3O_4NP exposure from 1 to 50 µg/ml. This enhanced cell mortality was also time-dependent (from day 2 to 6). The effects started early (i.e. already at day 2: - 20%) at lowest concentration (1 µg/ml) and increased (- 80%) at higher concentration (50 µg/ml). A worsening of cell death was evident over time (days 5 and 6) for the higher concentrations (≥ 25 µg/ml) (Fig. 12A). The control trend of spheroids in terms of cell viability and spheroid area during time (from day 2 to 6) was also reported (Fig. S1A). Extended cultivation of hNLC spheroids resulted in an increased cell loss associated to a decrease of the spheroid area starting at day 5 (Figure S1). This phenomenon could be clearly observed in Figure 3 (by light microscopy) showing the control spheroids at different time points (from day 2 to 10).

A concentration- and time-dependent decrease of ATP was also detected after Fe_3O_4NP exposure from 1 to 50 µg/ml from day 2 to 6. The effects (about 20% decrease content) started at day 2 and 10 µg/ml. After prolonged exposure (5-6 days) the effects were exacerbated (about 85% cell death from 25 µg/ml). No effects were observed at ≤ 5 µg/ml (Fig. 12B). The control value of ATP content as function of time is shown in Fig. S1B.

3.4.2. Morphology analysis

Fe_3O_4NPs (from 1 to 50 µg/ml) given at T0 induced disaggregation and area decrease of the spheroids, both effects were evidenced already at day 2 and from 5 µg/ml. Notably, at 25 µg/ml the disaggregation was relevant with many fragments. At 50 µg/ml, a complete disaggregation of the spheroids was evidenced (Fig. 13) and thus this concentration was not tested for the neuronal marker evaluation.

3.4.3. Fe_3O_4NP uptake

A marked time- and concentration-dependent Fe_3O_4NP uptake into hNLC spheroids was evidenced by Perls' Prussian blue staining. Spheroids showed an overload of NPs already at the lowest concentration tested (5 µg/ml) after 2 days from treatment which was further strengthened at the higher concentrations (10-25 µg/ml). Similar pattern was observed for hNLC spheroids after 6 days of NPs exposure. Notably, although fresh neurogenic medium (without Fe_3O_4NPs) was changed every 48 h for keeping cells healthy, Fe_3O_4NP internalization persisted over time (Fig. 14).

3.4.4. Neuronal marker evaluation

3.4.4.1. Immunofluorescence staining

Fe_3O_4NP treatments (from 1 to 25 µg/ml) affected the transdifferentiation of hMSCs into hNLC spheroids: a decrease of the fluorescence intensity was observed differently for each neuronal marker. Fe_3O_4NPs caused a fluorescence intensity decrease of both MAP-2 (green) and NSE (red) from day 2 at ≥ 10 µg/ml and from day 4 starting at lower concentration, 5 µg/ml (Figs. 15 and 16). Apparently, even 1 µg/ml caused a decrease fluorescence intensity after 5-6 days (Figs. 15 and 16). β-Tub III fluorescence intensity was apparently affected from day 4 and at the highest concentration tested (25 µg/ml Fe_3O_4NPs). After 5 days the effects started at 10 µg/ml. No effects at 1 µg/ml were observed (Fig. 17).
Black spots of Fe_3O_4NPs (in a dose-dependent manner) were also visible from the lowest concentration tested (1 µg/ml).
Notably, at 25 µg/ml, the spheroid disintegration began to be evident shortly after exposure (i.e. day 2) (Figs. 15, 16 and 17).

3.4.4.2 Flow cytometry

The evaluation of neuronal markers by flow cytometry in hNLC spheroids treated with Fe_3O_4NPs (5-10-25 µg/ml) starting from T0 of the neuronal induction and spheroid formation, indicated a significantly downregulation of the β-Tub III, MAP-2, and NSE proteins in a concentration-dependent manner, and starting early from day 2 (Fig. 18). β-Tub III and MAP-2 were downregulated from 5 µg/ml Fe_3O_4NPs and the effects exacerbated at 25 µg/ml. In particular, β-Tub III decreased at T2 from 28 to 47% (from 5 to 25 µg/ml) and remained low until day 6 (T6, decrease from 26 to 57%). MAP-2 was also similarly downregulated (about 20-50%).
The effect on NSE started at 10 µg/ml and persisted until day 6 (decrease about 30-60%). At T6 even the low concentration of 5 µg/ml started to decrease the marker (Fig. 18).

4 Discussion

The present study demonstrated for the first time that 3D spheroids of primary neuron-like cells of human origin can be generated from the differentiation of mesenchymal stem cells derived from human umbilical cord proving also that they can be useful for toxicity screening after short-term exposures to NPs.
During hNLC differentiation from hMSCs, spontaneous cell aggregation occurred using ULA 96-well round-bottomed plates. Additionally, conditions suitable to grow cell spheroids approximately 400-500 µm in diameter have been established. For all experiments, T0 spheroids were seeded starting with 25000 cells/well, since a consistent growth was detected until day 10. hNLCs also express neuronal markers such as β-Tub III, MAP-2, and NSE which increased from day 1 to 10 in parallel with the progression of hNLC spheroid differentiation. Additionally, the transdifferentiation of hMSCs into hNLCs was also supported by the downregulation, over time, of Nestin expression (typical marker of neural stem cells).
Whether Fe_3O_4NPs interfere with the neuronal differentiation process of hMSCs into hNLC spheroids was determined by evaluating two different time points of Fe_3O_4NPs application. In fact, spheroid formation time before exposure to NPs influenced the cell response, the outcome of the cell viability assays and neuronal markers expression. The following cytotoxicity tests, based on different principles for complementary information on Fe_3O_4NP toxicity, have been chosen: i) TB exclusion test, which is considered the standard method for estimating the cell population density (i.e. total number of living cells in the culture), and whose principle is based on live cells possessing intact cell membranes that exclude certain dyes, such as trypan blue, whereas dead cells do not. This test allows for a direct identification and quantification of live (unstained) and dead (blue) cells after the cell disaggregation of spheroids into a single cell suspension using trypsin solution (or

similar); and ii) bioluminescent ATP detection assay (commercial kit) based on ATP-dependent luciferase reaction occurring after the addition of lytic reagent and thus producing a luminescence signal proportional to the amount of cytosolic ATP present. The latter is in turn directly proportional to the number of viable cells. These cytotoxicity tests have been chosen to prevent Fe_3O_4NPs interference with classical *in vitro* cytotoxicity assays (e.g., MTT, MTS, Alamar blue and NRU assays) due to possible their interaction with the assay components in specific cell cultures. This phenomenon may thus result in read-out systems producing a wide array of false positives and false negatives (Costa et al., 2016; De Simone et al., 2020; Doak et al., 2009; Soenen & De Cuyper, 2009).
Finally, the flow cytometry analysis is particularly valuable as it can determine the amount of specific protein expressed within the cytoplasm of single cells in solution (McKinnon, 2018).

When Fe_3O_4NP exposure (a single treatment) was applied at the beginning of the transdifferentiation process (neurogenic induction) and simultaneously 3D forming (namely T0), a marked concentration- and time-dependent cell mortality was observed: the effect started early at very low concentration (i.e. 1 µg/ml) and exacerbated (80% mortality) after prolonged time (day 4-5-6) and increased concentrations (50 µg/ml). ATP content was also strikingly affected. Spheroid morphology was altered with disaggregation and fragmentation of the spheroids occurring early (day 2) from 5 µg/ml and culminating in a complete disaggregation of the spheroids at 50 µg/ml. Moreover, Fe_3O_4NP exposure also significantly downregulated β-Tub III, MAP-2, NSE differentiation proteins in a concentration-dependent manner starting at 5 µg/ml after day 2 which persisted up to day 6. In this type of early exposure to the challenger, spheroids showed an overload of NPs already at low concentration (5 µg/ml).

When the cells were allowed to form spheroids and Fe_3O_4NPs were administered at complete neuron 3D spheroid formation (namely after 4 days - T4), the adverse effects evaluated after short-term (24 (T5) and 48 (T6) h) exposure were less severe, compared to those obtained with the previous type of exposure, although cell mortality (from 20 to 60%) and decrease of ATP content (10-40%) were still observed in a concentration-dependent manner starting at 5 µg/ml. A size reduction (about 10%) of the spheroids was evidenced starting from 25 µg/ml after 24 h without morphology alteration. A neuronal-specific marker effect was also evidenced: MAP-2, the most affected, was significantly downregulated after 24 and 48 h exposure to Fe_3O_4NPs from 10 µg/ml; NSE decreased after 48 h exposure only, in a concentration-dependent manner, and β-Tub III decreased after 48 h at the highest concentration only, namely 50 µg/ml.
Specifically, in 3D fully formed spheroids (T4), cell-cell and cell-extracellular matrix (ECM) interactions seem to create a diffusion barrier for Fe_3O_4NPs uptake when these spheroids were treated at this time point. This phenomenon may have reduced the cytotoxic effects induced by Fe_3O_4NPs after 24-48 h exposure. On the other hand, when the cells were seeded at T0 directly with Fe_3O_4NPs, the cell-cell/cell-ECM interactions were more likely inhibited due to direct and continuous cells-NPs interactions during spheroid formation. Consequently, the effects on spheroid formation following the T0 treatment were more pronounced compared to those evidenced in spheroids treated at T4 (fully formed).

Our data also showed an efficient uptake of Fe_3O_4NPs into hNLCs, although the negative Zp and the wide size distribution values (ranging from about 1200 to 1500 nm) seem to be indicative of Fe_3O_4NP agglomeration/aggregation into the medium that apparently did not preclude the Fe_3O_4NP penetration into hNLC spheroids, as corroborated by blue spots of NPs in histological sections using H&E and Pearls' Prussian blue staining.
A penetration of Fe_3O_4NPs into spheroids, was observed in both exposure types: a concentration- and time-dependent uptake was evidenced when hNLC spheroids were exposed to Fe_3O_4NPs at complete spheroid formation (T4), and an overload of NPs early (day 2) at the lowest concentration

(5 µg/ml) was observed when hNLC spheroids were treated at T0 of the neurogenic induction. Importantly, after both types of NP treatments (i.e., T4 and T0), before performing each different test including histological staining, the treated spheroids were washed with PBS to remove any residue of Fe_3O_4NP in the medium suspension.
In the case of Fe_3O_4NP treatment at T4, the sequential sections (from outer edge to inner spheroid region), of each single spheroid, clearly showed, that after 24 and 48 h exposure, Fe_3O_4NPs were located on the outer rim of the spheroids, as well as in the inner layer, in which the NPs arranged in an uneven distribution. In particular, the NPs, evidenced in the histological sections of the spheroids, were clearly bound on their outer layer since the not adhered/adsorbed NPs have been washed off. Moreover, the evidenced NPs penetration into the spheroids, in deeper layers, may be related to NPs of smaller size (Fleddermann et al., 2019; Ulusoy et al., 2016).
Regarding to T0-treated spheroids, a more pronounced NP uptake was observed compared to that evidenced in spheroids treated at T4. It should be underlined that at T0 the cells are simply arranged in suspension, self-organization state is just starting, and cell-cell and cell-matrix interactions are considerably very low. In this context, the simultaneous addition of NPs to the cells ensured that all cells made contact with the Fe_3O_4NPs. Consequently, the NPs applied at cell seeding resulted in an increase of the penetration into the whole spheroid including its central region. This cell-NP load, in the spheroid interior, could result from embedding of NPs in the ECM during spheroid formation poorly interfering with the spheroid assembly at least up to 10 µg/ml of Fe_3O_4NPs exposure.

Comparing the present data obtained on 3D hNLC spheroids with those obtained in 2D hNLCs (De Simone et al., 2020) with respect to viability test (Trypan blue), a more pronounced sensitivity to Fe_3O_4NP-induced toxicity was evidenced in 3D spheroid model compared to that obtained in the respective 2D cultures. Cell death evaluation after 24 and 48 h exposure to Fe_3O_4NPs indicated a more pronounced effect shortly after exposure (24 h) even starting at lower concentration (i.e., at 5 µg/ml in spheroids instead of 50 µg/ml in monolayer cultures). Moreover, when hNLCs, either spheroids or 2D cultures, were exposed to Fe_3O_4NPs a significantly downregulation of the β-Tub III, MAP-2, NSE proteins was observed once again starting at lower concentrations in spheroids compared to 2D cells: effects started at 5-10 µg/ml after day 2 which persisted up to day 6 in spheroids *versus* 25 µg/ml after 2-3 days in 2D cells (Coccini et al., 2020).

Interestingly, when comparing two different types of human neuron-like spheroids, namely hNLCs (primary cells applying in the present study) *versus* SH-SY5Y (cell line), a higher sensitivity of the former to NP exposure was still evidenced in relation to the viability data obtained after 24 and 48 h Fe_3O_4NP exposure (De Simone et al., 2018). It is interesting to point out that SH-SY5Y neuronal cell line due to its cancerous origin (neuroblastoma) could be less sensitive to harmful actions caused by different chemicals. For example, den Hollander et al. (2014) have demonstrated a lower cytotoxicity in SH-SY5Y cells after methamphetamine administration compare to that evidenced in primary neuronal cultures.
Nevertheless, primary human hepatocytes spheroids have been shown to be the most sensitive to acetaminophen toxicity when compared to spheroids established from other cell types (Zhou et al., 2019).

Notably, an increasing number of studies use primary cell cultures and recently, pluripotent stem cells (PSCs), to create *in vitro* systems for neurotoxicity and developmental neurotoxicity screenings. In the last years a lot of effort has also been devoted to develop new protocols for establishing human 3D neurospheres most of them used cell lines or induced PSC (iPSCs). Recent paper has developed a new 3D model system namely iPSC-derived 3D neurospheres obtained from a human iPSC line (Ctrl-2 generated from a healthy Caucasian female donor peripheral blood mononuclear cells- PBMCs) to evaluate several well-known compounds with or without neurotoxic effect (e.g., paraquat, acrylamide, or ibuprofen): the acute exposure revealed distinct susceptibility

profiles in a differentiation stage-dependent manner, demonstrating that this hiPSC-based 3D *in vitro* model could effectively serve for neurotoxicity evaluation (Kobolak et al., 2020). Other new models of 3D human brain spheroids, both monocellular and multicellular, derived from cell line (LUHMES) or iPSCs (CRL2097 human fibroblast), have been developed to be applied for the evaluation of some NPs relevant for drug delivery. The study supported the usefulness of these 3D novel models to characterize NP neurotoxicity by the identification of specific cell types of CNS affected by NPs (Leite et al., 2019).

There is growing evidence indicating that culturing cells in 3D can promote a more *in vivo*-like phenotype than the same cell type cultured in 2D. This is particularly true for example when considering hepatocyte function and expression of DMETs (Bell et al., 2018; Cox et al., 2020; Gaskell et al., 2016; Hurrell et al., 2019). These 3D cells show greater sensitivity to detect toxicity for known hepatotoxic compounds, when compared to 2D cultures. The improved metabolic activity for 3D spheroids compared to 2D monolayers may, at least in part, explain the greater sensitivity of 3D spheroids to detect known hepatotoxins at concentrations that are toxicologically relevant *in vivo* (Cox et al., 2020). Globally, while 3D culture seems to improve hepatic phenotypes, its effects on sensitivity to hepatotoxins remain unclear.

With respect to NPs and spheroids only few published studies have evaluated the effects of nanoparticles in both 2D and 3D cell cultures. For example, A549 cells have been shown to be more sensitive to ZnONPs and TiO_2NPs in 3D spheroids compared to 2D monolayer (Sambale et al., 2015). Again, when using NIH-3T3 cells, TiO_2NPs were not toxic in 2D cultures but affected cell-cell interaction during 3D spheroid formation. Only with ZnONPs no differences in the sensitivity of the NIH-3T3 cells (3D *vs* 2D) were observed.
However, different results are also present in literature for NPs and spheroids, Kim et al. (2014) revealed similar cell proliferation of A549 cells in 2D and 3D cell cultures treated with ZnONP, whereas molecular markers for oxidative stress were significantly reduced only in 2D cell culture (Kim et al., 2014). Cell viability in C6 rat glioma spheroids was not decreased in the presence of TiO_2NP (Yamaguchi et al., 2010). Lee and colleagues (2009) showed a reduced toxic effect in HepG2 spheroids for cadmium telluride (CdTe) and gold nanoparticles in comparison to the 2D cell culture (Lee et al., 2009).
The present study showed that low concentrations of Fe_3O_4NPs, between 1-5 μg/ml, were able to induce adverse effects in hNLC spheroids particularly evident in early stage during neurogenic induction, even if toxicity was observed when exposure occurred at complete neuron 3D spheroid formation.
The critical concentrations of Fe_3O_4NPs inducing *in vitro* neurotoxicity were consistent with levels detected in brain tissue (0.040-58 μg/g) and peripheral blood (350-375 μg/ml) of IONPs-exposed laboratory animals (i.e., mice, rats, rabbits), and associated to alteration of mitochondrial function, cell membrane damage, oxidative stress, inflammation, apoptosis, increase of cerebral neurotransmitters content, such as dopamine and norepinephrine, with related consequences, motor and memory deficits, and neurobehavioral (Askri et al., 2018; Chahinez et al., 2016; Dhakshinamoorthy et al., 2017; Liu et al., 2018; Manickam & Dhakshinamoorthy, 2018; Wang et al., 2010; Wu et al., 2013).
Examining tissues collected from Alzheimer's disease patients, high concentration of Fe_3O_4 was detected (Hautot et al., 2003), as previously hypothesized (Dobson, 2001), and magnetite nanosphere from exogenous source (Maher et al., 2016, 2019), were recently found in human brain, demonstrating a direct transport of the xenobiotic into the brain.
Our results demonstrated from one side that our human based 3D spheroid models, could be applied as a predicting tool in neurotoxicology, and on the other hand that, despite the wide IONP applications, information on their potential adverse effects are still insufficient, and particular attention must be posed on potential neurotoxic damage.

5 Conclusion

In order to predict neurotoxicological effects of compounds the use of *in vitro* 3D models derived from human MSCs, could be relevant, particularly if applied as a pre-screening, in a testing strategy. The data obtained with neuronal spheroid *in vitro* models, indicate potential neurotoxic effects of Fe_3O_4NPs, which need to be further clarified for a correct risk assessment.

Acknowledgments

This work was supported in part by the Ricerca Corrente funding scheme of the Ministry of Health, Italy.

Conflict of interests

The authors declare that there is no conflict of interests regarding the publication of this paper.

Availability of data and material

The authors declare that all data presented are publicly available upon request.

Authors' contribution

Conceptualization was performed by T. C.; experimental planning and design were performed by T. C. and U. D. S.; the experiments were performed by U. D. S., A. C. C., P. P. and E. B.; data analysis and statistics were performed by T. C., U. D. S., A. C. C., P. P. and F. C.; writing-original draft preparation was performed by T. C. and U. D. S.; writing-review and editing were performed by T. C., U. D. S., A. C. C., P. P., E. B., and F. C.; supervision by T. C. All authors have read and agreed to the published version of the manuscript.

Ethics approval

Samples of umbilical cords were obtained from full-term pregnant women during elective caesarean sections at the Hospital Fondazione IRCCS Policlinico San Matteo in Pavia (Collaborative Project 201600038067 between ICS Maugeri, Pavia and Department of Obstetrics and Gynecology, Hospital Fondazione IRCCS Policlinico San Matteo, Pavia) after approval by Internal Ethics Committee of the Hospital Fondazione IRCCS Policlinico San Matteo, Pavia, Italy (Prot. 20170001171, 28.03.2017). The study was conducted in accordance with the Helsinki Declaration.

Consent to participate

Informed consent was gained from each participant healthy donor mother at the Hospital Fondazione IRCCS Policlinico San Matteo in Pavia, Italy (from 2017 to 2019) (Prot. 20170001171, 28.03.2017).

Consent for publication

Consent for scientific publication was gained from the mothers preserving their privacy, confidentiality and anonymity.

References

Akbarzadeh, A., Samiei, M., & Davaran, S. (2012). Magnetic nanoparticles: preparation, physical properties, and applications in biomedicine. *Nanoscale Research Letters*, *7*, 144. https://doi.org/10.1186/1556-276x-7-144.

Askri, D., Ouni, S., Galai, S., Arnaud, J., Chovelon, B., Lehmann, S.G., … Amara, S. (2018). Intranasal instillation of iron oxide nanoparticles induces inflammation and perturbation of trace elements and neurotransmitters, but not behavioral impairment in rats. *Environmental Science and Pollution Research International, 25*, 16922-16932. https://doi.org/10.1007/s11356-018-1854-0.

Bai, C., & Tang, M. (2020). Toxicological study of metal and metal oxide nanoparticles in zebrafish. *Journal of Applied Toxicology*, *40*, 37-63. https://doi.org/10.1002/jat.3910.

Bal-Price, A., Pistollato, F., Sachana, M., Bopp, S. K., Munn, S., & Worth, A. (2018). Strategies to improve the regulatory assessment of developmental neurotoxicity (DNT) using in vitro methods. *Toxicology and Applied Pharmacology*, *354*, 7-18. https://doi.org/10.1016/j.taap.2018.02.008.

Bell C. C., Dankers, A. C. A., Lauschke, V. M., Sison-Young, R., Jenkins, R., Rowe, C., Goldring, C. E., … Ingelman-Sundberg, M. (2018). Comparison of hepatic 2D sandwich cultures and 3D spheroids for long-term toxicity applications: a multicenter study. *Toxicological Sciences*, *162*, 655-666. https://doi.org/10.1093/toxsci/kfx289.

Bongaerts, E. S., Nawrot, T., van Pee, T., Ameloot, M., & Bové, H. (2020). Translocation of (ultra)fine particles and nanoparticles across the placenta; a systematic review on the evidence of in vitro, ex vivo, and in vivo studies. *Particle and Fibre Toxicology*, *17*, 56. https://doi.org/10.1186/s12989-020-00386-8.

Cesarz, Z., & Tamama, K. (2016). Spheroid culture of mesenchymal stem cells. *Stem Cells International*, *2016*, 9176357. http://dx.doi.org/10.1155/2016/9176357.

Chahinez, T., Rachid, R., Salim, G., Lamia, B., Ghozala, Z., Nadjiba, T., … Belgacem, D. (2016). Toxicity of Fe_3O_4 nanoparticles on oxidative stress status, stromal enzymes and mitochondrial respiration and swelling of Oryctolagus cuniculus brain cortex. *Toxicology and Environmental Health Sciences*, *8*, 349-355. Doi: 10.1007/s13530-016-0296-7.

Chang, X. Li, J., Niu, S., Xue, Y., & Tang, M. (2021). Neurotoxicity of metal-containing nanoparticles and implications in glial cells. *Journal of Applied Toxicology*, *41*(1), 65-81. https://doi.org/10.1002/jat.4037.

Coccini, T., De Simone, U., Roccio, M., Croce, S., Lenta, E., Zecca, M., Spinillo, A., & Avanzini, M.A. (2019). In vitro toxicity screening of magnetite nanoparticles by applying mesenchymal stem cells derived from human umbilical cord lining. *Journal of Applied Toxicology*, *39*, 1320-1336. https://doi.org/10.1002/jat.3819.

Coccini, T., Pignatti, P., Spinillo, A., & De Simone, U. (2020). Developmental neurotoxicity screening for nanoparticles using neuron-like cells of human umbilical cord mesenchymal stem cells: example with magnetite nanoparticles. *Nanomaterials (Basel)*, *10*(8), 1607. https://doi.org/10.3390/nano10081607.

Cortés-Medina, L. V., Pasantes-Morales, H., Aguilera-Castrejon, A., Picones, A., Lara-Figueroa, C. O., Luis, E., … Ramos-Mandujano, G. (2019). Neuronal transdifferentiation potential of human mesenchymal stem cells from neonatal and adult sources by a small molecule cocktail. *Stem Cells International*, 7627148. https://doi.org/10.1155/2019/7627148.

Costa, C., Brandão, F., Bessa, M. J., Costa, S., Valdiglesias, V., Kiliç, G., … Teixeira, J. P. (2016). In vitro cytotoxicity of superparamagnetic iron oxide nanoparticles on neuronal and glial cells. Evaluation of nanoparticle interference with viability tests. *Journal Applied Toxicology*, *36*(3), 361-372. doi: 10.1002/jat.3213.

Cox, C. R., Lynch, S., Goldring, C., & Sharma, P. (2020). Current perspective: 3D spheroid models utilizing human-based cells for investigating metabolism-dependent drug-induced liver injury. *Frontiers in Medical Technology*, *2*, 611913 https://doi.org/10.3389/fmedt.2020.611913.

Cupaioli, F. A., Zucca, F. A., Boraschi, D., & Zecca, L. (2014). Engineered nanoparticles. How brain friendly is this new guest? *Progress in Neurobiology, 119-120*, 20-38. https://doi.org/10.1016/j.pneurobio.2014.05.002.

Czarnecka, J., Porowińska, D., Bajek, A., Hołysz, M., & Roszek, K. (2017). Neurogenic differentiation of mesenchymal stem cells induces alterations in extracellular nucleotides metabolism. *Journal of Cellular Biochemistry*, *118*, 478-486. https://doi.org/10.1002/jcb.25664.

den Hollander, B., Sundström, M., Pelander, A., Ojanperä, I., Mervaala, E., Korpi, E. R., & Kankuri, E. (2014). Keto amphetamine toxicity-focus on the redox reactivity of the cathinone designer drug mephedrone. *Toxicological Sciences*, *141*(1), 120-131. https://doi.org/10.1093/toxsci/kfu108.

De Simone, U., Roccio, M., Gribaldo, L., Spinillo, A., Caloni, F., & Coccini, T. (2018). Human 3D cultures as models for evaluating magnetic nanoparticle CNS cytotoxicity after short- and repeated long-term exposure. *International Journal of Molecular Sciences*, *19*(7), 1993. https://doi.org/10.3390/ijms19071993.

De Simone, U., Spinillo, A., Caloni, F., Gribaldo, L., & Coccini, T. (2020). Neuron-like cells generated from human umbilical cord lining-derived mesenchymal stem cells as a new in vitro model for neuronal toxicity screening: using magnetite nanoparticles as an example. *International Journal of Molecular Sciences*, *21*(1), 271. https://doi.org/10.3390/ijms21010271.

De Simone, U., Spinillo, A., Caloni, F., Avanzini, M. A., & Coccini T. (2020). In vitro evaluation of magnetite nanoparticles in human mesenchymal stem cells: comparison of different cytotoxicity assays. *Toxicology Mechanisms & Methods*, *30*(1), 48-59. doi: 10.1080/15376516.2019.1650151.

Dhakshinamoorthy, V., Manickam, V., & Perumal, E. (2017). Neurobehavioral toxicity of iron oxide nanoparticles in mice. *Neurotoxicity Research*, *32*, 187-203. https://doi.org/10.1007/s12640-017-9721-1.

Doak, S. H., Griffiths, S. M., Manshian, B., Singh, N., Williams, P. M., Brown, A. P., & Jenkins G. J. (2009). Confounding experimental considerations in nanogenotoxicology. *Mutagenesis*, *24*(4), 285-293. doi: 10.1093/mutage/gep010.

Djurisic, A. B., Leung, Y. H., Ng, A. M., Xu, X. Y., Lee, P. K., Degger, N., & Wu, R. S. S. (2015). Toxicity of metal oxide nanoparticles: Mechanisms, characterization, and avoiding experimental artefacts. *Small*, *11*(1), 26-44. https://doi.org/10.1002/smll.201303947.

Dobson, J. (2001). Nanoscale biogenic iron oxides and neurodegenerative disease. *FEBS LETTERS*, *496*, 1-5. https://doi.org/10.1016/s0014-5793(01)02386-9.

Fleddermann, J., Susewind, J., Peuschel, H., Koch, M., Tavernaro, I., & Kraegeloh, A. (2019). Distribution of SiO_2 nanoparticles in 3D liver microtissues. *International Journal of Nanomedicine*, *22*, 14:1411-1431. doi: 10.2147/IJN.S189888.

Gaskell, H., Sharma, P., Colley, H. E., Murdoch, C., Williams, D. P., & Webb, S. D. (2016). Characterization of a functional C3A liver spheroid model. *Toxicology Research*, *5*, 1053-1065. https://doi.org/10.1039/c6tx00101g.

Gibb, S. (2008). Toxicity testing in the 21st century: a vision and a strategy. *Reproductive Toxicology*, *25*(1), 136-138. http://www.ncbi.nlm.nih.gov/pubmed/18093799.

Goodman, T. T., Ng, C. P., & Pun, S. H. (2008). 3-D tissue culture systems for the evaluation and optimization of nanoparticle-based drug carriers. *Bioconjugate Chemistry*, *19*(10), 1951-1959. http://www.ncbi.nlm.nih.gov/pubmed/18788773.

Gottardo, S., Mech, A., Drbohlavová, J., Małyska, A., Bøwadt, S., Riego Sintes, J., & Rauscher, H. (2021). Towards safe and sustainable innovation in nanotechnology: State-of-play for smart nanomaterials. *NanoImpact*, *21*, 100297. http://10.1016/j.impact.2021.100297.

Handral, H. K., Tong, H. J., Islam, I., Sriram, G., Rosa, V., & Cao, T. (2016). Pluripotent stem cells: an in vitro model for nanotoxicity assessments. *Journal of Applied Toxicology*, *36*, 1250-1258. https://doi.org/10.1002/jat.3347.

Hautot, D., Pankhurst, Q. A., Khan, N., & Dobson, J. (2003). Preliminary evaluation of nanoscale biogenic magnetite in Alzheimer's disease brain tissue. *Proceedings Biological Sciences*, *270*, S62-S64. https://doi.org/10.1098/rsbl.2003.0012.

Hernández, R., Jiménez-Luna, C., Perales-Adán, J., Perazzoli, G., Melguizo, C., & Prados, J. (2020). Differentiation of human mesenchymal stem cells towards neuronal lineage: clinical trials in nervous system disorders. *Biomolecules & Therapeutics*, *28*(1), 34-44. https://doi.org/10.4062/biomolther.2019.065.

Hoelting, L., Scheinhardt, B., Bondarenko, O., Schildknecht, S., Kapitza, M., Tanavde, V., … Kadereit, S. (2013). A 3-dimensional human embryonic stem cell (hESC)-derived model to detect developmental neurotoxicity of nanoparticles. *Archives of Toxicology*, *87*(4), 721-733. http://www.ncbi.nlm.nih.gov/pubmed/23203475.

Hu, Y., & Gao, J. (2010). Potential neurotoxicity of nanoparticles. *International Journal of Pharmaceutics*, *394*(1-2), 115-121. https://doi.org/10.1016/j.ijpharm.2010.04.026.

Hurrell, T., Lilley, K. S., & Cromarty, A. D. (2019). Proteomic responses of HepG2 cell monolayers and 3D spheroids to selected hepatotoxins. *Toxicology Letters*, *300*, 40-50. https://doi.org/10.1016/j.toxlet.2018.10.030.

Joshi, P., Kang, S. Y., Yu, K. N., Kothapalli, C., & Lee, M. Y. (2020). High-content imaging of 3D-cultured neural stem cells on a 384-pillar plate for the assessment of cytotoxicity. *Toxicology in Vitro*, *65*, 104765, https://doi.org/10.1016/j.tiv.2020.104765.

Jurga, M., Lipkowski, A. W., Lukomska, B., Buzanska, L., Kurzepa, K., Sobanski, T., … Domanska-Janik, K. (2009). Generation of functional neural artificial tissue from human umbilical cord blood stem cells. *Tissue Engineering Part C, Methods*, *15*(3), 365-372. http://www.ncbi.nlm.nih.gov/pubmed/19719393.

Kil, K., Choi, M. Y., & Park, K. H. (2016). In vitro differentiation of human wharton's jelly-derived mesenchymal stem cells into auditory hair cells and neurons. *Journal of International Advanced Otology*, *12*, 37-42. https://doi.org/10.5152/iao.2016.1190.

Kim, E., Jeon, W. B., Kim, S., & Lee, S. K. (2014). Decrease of reactive oxygen species-related biomarkers in the tissue-mimic 3D spheroid culture of human lung cells exposed to zinc oxide nanoparticles. *Journal of Nanoscience and Nanotechnology*, *14*(5), 3356-3365. https://doi.org/10.1166/jnn.2014.8257.

Kim, T. W., Che, J. H., & Yun, J. W. (2019). Use of stem cells as alternative methods to animal experimentation in predictive toxicology. *Regulatory Toxicology and Pharmacology*, *105*, 15-29. https://doi.org/10.1016/j.yrtph.2019.03.016.

Kobolak, J., Teglasi, A., Bellak, T., Janstova, Z., Molnar, K., Zana, M., … Dinnyes, A. (2020). Human induced pluripotent stem cell-derived 3d-neurospheres are suitable for neurotoxicity screening. *Cells*, *9*(5), 1122. https://doi.org/10.3390/cells9051122.

Knudsen, T. B., Keller, D. A., Sander, M., Carney, E. W., Doerrer, N. G., Eaton, D. L., … Whelan, M. (2015). FutureTox II: in vitro data and in silico models for predictive toxicology. *Toxicological Sciences*, 143, 256-267. https://doi.org/10.1093/toxsci/kfu234.

Landrigan, P.J., & Miodovnik, A. (2011). Children's health and the environment: An overview. *Mount Sinai Journal of Medicine*, *78*, 1-10. https://doi.org/10.1002/msj.20236.

Langhans, S. A. (2018). Three-dimensional in vitro cell culture models in drug discovery and drug repositioning. *Frontiers in Pharmacology*, *9*, 6. https://doi.org/10.3389/fphar.2018.00006.

Lee, J., Lilly, G. D., Doty, R. C., Podsiadlo, P., & Kotov, N. A. (2009). In vitro toxicity testing of nanoparticles in 3D cell culture. *Small*, *5*(10), 1213-1221. http://www.ncbi.nlm.nih.gov/pubmed/19263430.

Lee, S. J., & Lee, H. A. (2020). Trends in the development of human stem cell-based non-animal drug testing models. *Korean Journal of Physiology & Pharmacology*, *24*(6), 441-452. https://doi.org/10.4196/kjpp.2020.24.6.441.

Leite, P. E. C., Pereira, M. R., Harris, G., Pamies, D., Gobbo Dos Santos, L. M., Granjeiro, J. M., … Smirnova, L. (2019). Suitability of 3D human brain spheroid models to distinguish toxic effects of gold and poly-lactic acid nanoparticles to assess biocompatibility for brain drug delivery. *Particle and Fibre Toxicology*, *6*, 22. https://doi.org/10.1186/s12989-019-0307-3.

Liu, Y., Li, J., Xu, K., Gu, J., Huang, L., Zhang, L., … Zhang, L. (2018). Characterization of superparamagnetic iron oxide nanoparticle-induced apoptosis in PC12 cells and mouse

hippocampus and striatum. *Toxicology Letters*, *292*, 151-161. https://doi.org/10.1016/j.toxlet.2018.04.033.

Maher, B. A., Ahmed, I. A., Karloukovski, V., MacLaren, D. A., Foulds, P. G., Allsop, D., … Calderon-Garciduenas, L. (2016). Magnetite pollution nanoparticles in the human brain. *Proceedings of the National Academy of Sciences of the United States of America*, *113*, 10797-10801. https://doi.org/10.1073/pnas.1605941113.

Maher, B. A. (2019). Airborne magnetite and iron-rich pollution nanoparticles: potential neurotoxicants and environmental risk factors for neurodegenerative disease, including Alzheimer's disease. *Journal of Alzheimer's Disease*, *71*, 361-375. https://doi.org/10.3233/jad-190204.

Manickam, V., & Dhakshinamoorthy, V. (2018). Perumal E. Iron oxide nanoparticles induces cell cycle dependent neuronal apoptosis in mice. *Journal of Molecular Neuroscience*, *64*, 352-362. https://doi.org/10.1007/s12031-018-1030-5.

McKinnon, K. M. (2019). Flow Cytometry: An Overview. *Current Protocols in Immunology*, *120*, 5.1.1-5.1.11. doi:10.1002/cpim.40.

National Research Council (NRC). (2007). Toxicity testing in the 21*st* century: a vision and a strategy. Washington, DC: The National Academies Press. https://doi.org/10.17226/11970.

Pamies, D., Hartung, T., & Hogberg, H. T. (2014). Biological and medical applications of a brain-on-a-chip. *Experimental Biology and Medicine*, *239*(9), 1096-1107. http://www.ncbi.nlm.nih.gov/pubmed/24912505.

Petros, R. A., & DeSimone, J. M. (2010). Strategies in the design of nanoparticles for therapeutic applications. *Nature Reviews Drug Discovery*, *9*, 615-627. https://doi.org/10.1038/nrd2591.

Raileanu, V. N., Whiteley, J., Chow, T., Kollara, A., Mohamed, A., Keating, A., & Rogers, I. M. (2019). Banking mesenchymal stromal cells from umbilical cord tissue: large sample size analysis reveals consistency between donors. *Stem Cells Translational Medicine*, *8*(10), 1041-1054. doi: 10.1002/sctm.19-0022. https://doi.org/10.1002/sctm.19-0022.

Rowatt, K., Burns, R. E., Frasca, S. Jr., & Long, D. M. (2018). A combination Prussian blue - hematoxylin and eosin staining technique for identification of iron and other histological features. *Journal of Histotechnology*, *41*(1), 29-34. https://doi.org/10.1080/01478885.2017.1417696.

Sambale, F., Lavrentieva, A., Stahl, F., Blume, C., Stiesch, M., Kasper, C., Bahnemann, D., & Scheper, T. (2015). Three dimensional spheroid cell culture for nanoparticle safety testing. *Journal of Biotechnology*, *205*,120-129. https://doi.org/10.1016/j.jbiotec.2015.01.001.

Sambuy, Y., Alloisio, S., Bertanza, G., Ferretti, D., Letasiova, S., Mazzoleni, G., Pedrazzani, R., & Caloni, F. (2018). Air, water and soil: Which alternatives? Alternative models in environmental toxicology. *ALTEX*, *35*, 254-256. https://doi.org/10.14573/altex.1802121.

Shahbazi, A., Safa, M., Alikarami, F., Kargozar, S., Asadi, M. H., Joghataei, M. T., & Soleimani, M. (2016). Rapid induction of neural differentiation in human umbilical cord matrix

mesenchymal stem cells by camp-elevating agents. *International Journal of Molecular and Cellular Medicine*, *5*, 167-177.

Shi, D., Mi, G., Bhattacharya, S., Nayar, S., & Webster, T. J. (2016). Optimizing superparamagnetic iron oxide nanoparticles as drug carriers using an in vitro blood-brain barrier model. *International Journal of Nanomedicine*, *11*, 5371-5379. https://doi.org/10.2147/ijn.s108333.

Shi, Y., Nan, C., Yan, Z., Liu, L., Zhou, J., Zhao, Z., & Li, D. (2018). Synaptic plasticity of human umbilical cord mesenchymal stem cell differentiating into neuron-like cells in vitro induced by edaravone. *Stem Cells International*, *5304279*. https://doi.org/10.1155/2018/5304279.

Singh, S., Srivastava, A., Kumar, V., Pandey, A., Kumar, D., Rajpurohit, C.S., … Pant, A. B. (2015). Stem cells in neurotoxicology/developmental neurotoxicology: Current scenario and future prospects. *Molecular Neurobiology*, *53*, 6938-6949. https://doi.org/10.1007/s12035-015-9615-2.

Singh, A. K., & Kashyap, M. P. (2016). An overview on human umbilical cord blood stem cell-based alternative in vitro models for developmental neurotoxicity. *Molecular Neurobiology*, *53*, 3216-3226. https://doi.org/10.1007/s12035-015-9202-6.

Sly, P. D., & Flack, F. (2008). Susceptibility of children to environmental pollutants. *Annals of the New York Academy of Sciences*, *1140*, 163-183. https://doi.org/10.1196/annals.1454.017.

Soenen, S. J., & De Cuyper M. (2009). Assessing cytotoxicity of (iron oxidebased) nanoparticles: an overview of different methods exemplified with cationic magnetoliposomes. *Contrast Media & Molecular Imaging*, *4*(5), 207-219. doi: 10.1002/cmmi.282.

Sreekanthreddy, P., Gromnicova, R., Davies, H., Phillips, J., Romero, I. A., & Male, D. (2015). A three-dimensional model of the human blood-brain barrier to analyse the transport of nanoparticles and astrocyte/endothelial interactions. *F1000 Research*, *4*,1279. http://www.ncbi.nlm.nih.gov/pubmed/26870320.

Stueckle, T. A., & Roberts, J. R. R. (2019). Perspective on current alternatives in nanotoxicology research. *Applied In Vitro Toxicology*, *5*, 3. https://doi.org/10.1089/aivt.2019.29020.jrr.

Suma, R. N., & Mohanan, P. V. (2015). Stem cells, a new generation model for predictive nanotoxicological assessment. *Current Drug Metabolism*, *16*, 932-939. https://doi.org/10.2174/1389200216666151015113720.

Tukker, A. M., De Groot, M. W. G. D. M., Wijnolts, F. M. J., Kasteel, E. E. J., Hondebrink, L., & Westerink, R. H. S. (2016). Research article is the time right for in vitro neurotoxicity testing using human iPSC-derived neurons? *ALTEX*, *33*, 261-271. https://doi.org/10.14573/altex.1510091.

Ulusoy, M., Lavrentieva, A., Walter, J. G., Sambale, F., Green, M., Stahl, F., & Scheper, T. (2016). Evaluation of CdTe/CdS/ZnS core/shell/shell quantum dot toxicity on three-dimensional spheroid cultures. *Toxicology Research*, *5*(1), 126-135. doi: 10.1039/c5tx00236b.

Wang, J., Chen, Y., Chen, B., Ding, J., Xia, G., Gao, C., … Wang, X. M. (2010). Pharmacokinetic parameters and tissue distribution of magnetic Fe_3O_4 nanoparticles in mice. *International Journal of Nanomedicine*, *5*, 861-866. https://doi.org/10.2147/ijn.s13662.

Wang, Y., Xiong, L., & Tang, M. (2017). Toxicity of inhaled particulate matter on the central nervous system: Neuroinflammation, neuropsychological effects and neurodegenerative disease. *Journal of Applied Toxicology*, *37*, 644-667. https://doi.org/10.1002/jat.3451.

Wang, Y., & Tang, M. (2018). Review of in vitro toxicological research of quantum dot and potentially involved mechanisms. *Science of the Total Environment*, (625), 940-962. https://doi.org/10.1016/j.scitotenv.2017.12.334.

Willmann, W., & Dringen, R. (2019). How to study the uptake and toxicity of nanoparticles in cultured brain cells: The dos and don't forgets. *Neurochemical Research*, *44*, 1330-1345. https://doi.org/10.1007/s11064-018-2598-4.

Win-Shwe, T., & Fujimaki, H. (2011). Nanoparticles and neurotoxicity. *International Journal of Molecular Sciences*, *12*, 6267-6280.

Wu, J., Ding, T., & Sun, J. (2013). Neurotoxic potential of iron oxide nanoparticles in the rat brain striatum and hippocampus. *NeuroToxicology*, *34*, 243-253. https://doi.org/10.1016/j.neuro.2012.09.006.

Wu, T., & Tang, M. (2018). Review of the effects of manufactured nanoparticles on mammalian target organs. *Journal of Applied Toxicology*, *38*(1), 25-40. https://doi.org/10.1002/jat.3499.

Yamaguchi, S., Kobayashi, H., Narita, T., Kanehira, K., Sonezaki, S., Kubota, Y., Terasaka, S., & Iwasaki, Y. (2010). Novel photodynamic therapy using water-dispersed TiO_2-polyethylene glycol compound: evaluation of antitumor effect on glioma cells and spheroids in vitro. *Photochemistry and Photobiology*, *86*(4), 964-971. https://doi.org/10.1111/j.1751-1097.2010.00742.x.

Zeng, Y., Kurokawa, Y., Zeng, Q., Win-Shwe, T. T., Nansai, H., Zhang, Z., & Sone, H. (2016). Effects of polyamidoamine dendrimers on a 3-D neurosphere system using human neural progenitor cells. *Toxicological Sciences*, *152*(1), 128-144. http://www.ncbi.nlm.nih.gov/pubmed/27125967.

Zhou, Y., Shen, J. X., & Lauschke, V. M. (2019). Comprehensive evaluation of organotypic and microphysiological liver models for prediction of drug-induced liver injury. *Frontiers in Pharmacology*, *10*, 1093. https://doi.org/10.3389/fphar.2019.01093.

Legends to Figures

Fig. 1. Exposure approach. Schematic overview depicting the design of the two Fe_3O_4NP exposure approaches and endpoints applied in this study. In the first approach the hNLC spheroids were treated with increasing concentrations of Fe_3O_4NPs at day 4 (T4) of the neurogenic induction; in the second approach, hNLCs were treated with Fe_3O_4NPs at time T0 of both spheroid formation and neurogenic differentiation.

Fig. 2. Physico-chemical properties of the Fe_3O_4NPs in culture medium. Size distribution of the Fe_3O_4NP suspensions at 10 and 25 µg/ml in neurogenic medium after 24 and 48 h evaluated by dynamic light scattering. The tables summarize the physico-chemical properties of the Fe_3O_4NP suspension. Zp, zeta potential; Pdl, polydispersity index.

Fig. 3. Characterization of hNLC spheroids over time at different cell numbers seeded. Representative images of hNLCs spheroids in 96 ULA plate seeded at the cell density indicated in the figure during time (from day 2 to day 10). The graphic/plot shows the size (area) of hNLC spheroids at different cell density for each time point considered. Table summarizes the morphological changes observed over time for each cell density.

Fig. 4. hNLC spheroid sections over time after H&E staining. No difference in morphology was observed during time: hNLC spheroids showed a well-defined circular structure. The cells on the outside were elongated compared to those on the inside formed by triangular-shaped cells with a round nucleus. Necrotic core or hypoxia, in term of reduced cell density, apoptotic nuclei and lighter eosin staining, was not evidenced. No necrotic core or hypoxia was present. The cells were seeded at 25000 cells/well, and hNLC spheroids were cultured up to 10 days. It has been advocated the use of at least 18-24 replicates per condition as spheroids can be lost during feeding or transfer. Diameter was expressed as mean ± S.E. Scale Bar 50 µm.

Fig. 5. Immunofluorescence analysis of the neuronal marker expression in hNLC spheroids. Representative fluorescence merged images of hNLC spheroid sections labelled for β-Tub III (structural marker, green), MAP-2 (mature neuron marker, green) and NSE (cytoplasmic protein expressed by mature neuron, red). The fluorescence pattern of each neuronal marker in hNLC spheroids cultured in neurogenic medium increased from day 2 to day 10. Nuclei were counterstained with Hoechst 33258. Scale bar: 100 µm.

Fig. 6. Flow cytometry analysis of the neuronal marker expression in hNLC spheroids. Neuronal marker expression (β-Tub III, MAP-2, NSE, Nestin) was evaluated during time from day 1 to day 10. Data are expressed as MFI and represent the mean ± S.E. * $p < 0.05$, statistical analysis by ono-way ANOVA followed by Tukey's multiple comparisons test.

Fig. 7. Cytotoxicity effects after Fe_3O_4NPs exposure in hNLC spheroids treated at T4. Cell viability evaluation by Trypan blue (TB) exclusion test (A) and ATP content evaluation (B) in hNLC spheroids treated with increasing concentration of Fe_3O_4NPs (5-100 µg/ml) for 24 and 48 h exposure. Data are normalized to the mean value obtained under control condition and expressed as percentage (% of each control) and plotted as the mean ± S.E. * $p < 0.05$, statistical analysis by one-way ANOVA followed by Tukey's multiple comparisons test.

Fig. 8. hNLC spheroid growth treated at T4. Morphological analysis (A) and spheroid area estimation (B) of the hNLC spheroids treated at T4 and evaluated after 24 and 48 h exposure to increasing Fe_3O_4NP concentrations (5-100 µg/ml). No morphological alteration was observed after Fe_3O_4NP exposure. The calculated area revealed that Fe_3O_4NP treatments resulted in reduction

starting from 25 µg/ml already after 24 h without exacerbation after 48 h. hNLC spheroid area was calculated by Image J software. Data are normalized to the mean value obtained under control condition (area of control at 24 h: 0.171 ± 0.004 mm^2; area of control at 48 h: 0.163 ± 0.007 mm^2) and expressed as mean ± S.E. Scale Bar: 100 µm.

Fig. 9. Fe_3O_4NP uptake in hNLCs treated at T4. Qualitative evaluation of Fe_3O_4NPs uptake using Perls' Prussian blue staining in hNLC spheroids treated with increasing concentration of Fe_3O_4NPs (10-50 µg/ml) at T4 for 24 and 48 h exposure. Fe_3O_4NP uptake into hNLC spheroids was concentration- and time-dependent as showed in representative micrographs of hNLC spheroid sections. Fe_3O_4NPs, at the lowest concentration tested, were visible on the surface and in the outer layers of the spheroid; at the higher Fe_3O_4NP concentrations (25-50 µg/ml) and continuing with the exposure (48 h), Fe_3O_4NPs were observed in the inner layers of spheroids reaching also the core of hNLC spheroids. Scale Bar: 50 µm.

Fig. 10. Immunofluorescence analysis of neuronal markers in hNLCs treated at T4. Representative fluorescence merged images of hNLC spheroid sections after 24 (A) and 48 h (B) exposure with increasing concentration of Fe_3O_4NPs (10-50 µg/ml). A reduction of the MAP-2 and NSE fluorescence pattern at 50 µg/ml and 25 µg/ml respectively was visible after 24 h exposure and for both at 25 µg/ml after 48 h. While, a decrease β-Tub III fluorescence was observed after 48 h only. Scale Bar: 100 µm.

Fig. 11. Flow cytometry analysis of the neuronal marker expression in hNLC spheroids treated at T4. Neuronal marker expression (β-Tub III, NSE, MAP-2) was evaluated after 24 and 48 h exposure to increasing concentration of Fe_3O_4NPs (10-50 µg/ml). Data are expressed as MFI percentage (% of respective control) and plotted as the mean ± S.E. * $p < 0.05$, statistical analysis by ono-way ANOVA followed by Tukey's multiple comparisons test.

Fig. 12 Cytotoxicity effects after Fe_3O_4NPs exposure in hNLC spheroids treated at T0. Cell viability evaluation by Trypan blue (TB) exclusion test (A) and ATP content evaluation (B) in hNLC spheroids treated with increasing concentration of Fe_3O_4NPs (1-50 µg/ml) at T0. The assessments were performed at day 2, 3, 5, 6. Data are normalized to the mean value obtained under control conditions and expressed as percentage (% of each control) and plotted as the mean ± S.E. * $p < 0.05$, statistical analysis by one-way ANOVA followed by Tukey's multiple comparisons test.

Fig. 13. hNLC spheroid growth treated at T0. Morphological analysis (A) and spheroid area estimation (B) of the hNLC spheroids treated at T0 with increasing Fe_3O_4NP concentrations (1-50 µg/ml). hNLC spheroids displayed loss of compactness, together with loose cells on periphery associated with an area reduction starting from 5 µg/ml already at day 2 with exacerbation at higher concentrations and persisting up to day 6.
hNLC spheroid area was calculated by Image J software. Data were normalized to the mean value obtained under control conditions (area of control at day 2: 0.165 ± 0.0003 mm^2; area of control at day 3: 0.169 ± 0.002 mm^2; area of control at day 5: 0.170 ± 0.001 mm^2; area of control at day 6: 0.124 ± 0.001 mm^2) and expressed as mean ± S.E. Scale Bar 100 µm.

Fig. 14. Fe_3O_4NP uptake after T0 treatment. Qualitative evaluation of Fe_3O_4NPs uptake using Perls' Prussian blue staining in hNLC spheroids treated with increasing concentration of Fe_3O_4NPs (5-25 µg/ml) at T0. The representative images of hNLC spheroid sections indicated that Fe_3O_4NPs were immediately detectable in the core of hNLC spheroids already at day 2. An overload of NPs was observed already at the lowest concentration tested (5 µg/ml), increased at the higher concentrations (10-25 µg/ml), and persisted up to day 6. Scale Bar 50 µm.

Fig. 15. Immunofluorescence analysis of MAP-2 in hNLCs treated at T0. Representative fluorescence merged microphotographs of hNLC spheroid sections showing the Fe_3O_4NP effects on MAP-2 (Microtubule-associated protein 2). The fluorescence decrease started from 10 µg/ml already at day 2 with exacerbation during time. Nuclei were counterstained with Hoechst 33258. Scale Bar: 100 µm.

Fig. 16. Immunofluorescence analysis of NSE in hNLCs treated at T0. Representative fluorescence merged microphotographs of hNLC spheroid sections showing the Fe_3O_4NP effects on NSE (enolase) expression. The fluorescence decrease started from 10 µg/ml already at day 2 with a strong exacerbation at lowest concentration (≥ 1 µg/ml) tested at day 5 and day 6. Nuclei were counterstained with Hoechst 33258. Scale Bar: 100 µm.

Fig. 17. Immunofluorescence analysis of β-Tub III in hNLCs treated at T0. Representative fluorescence merged microphotographs of hNLC spheroid sections showing the Fe_3O_4NP effects on β-Tub III. A reduction of fluorescence was observed from day 4 at the highest concentration tested (25 µg/ml) with exacerbation at day 5 and day 6. Nuclei were counterstained with Hoechst 33258. Scale Bar: 100 µm.

Fig. 18. Flow cytometry analysis of the neuronal marker expression in hNLC spheroids treated at T0. Neuronal marker expression (β-Tub III, NSE, MAP-2) in hNLC spheroids treated with increasing concentration of Fe_3O_4NPs (1-25 µg/ml) was evaluated at T0 and at different time points. Data are expressed as MFI percentage (% of respective control) and plotted as the mean ± S.E. * $p < 0.05$, statistical analysis by ono-way ANOVA followed by Tukey's multiple comparisons test.

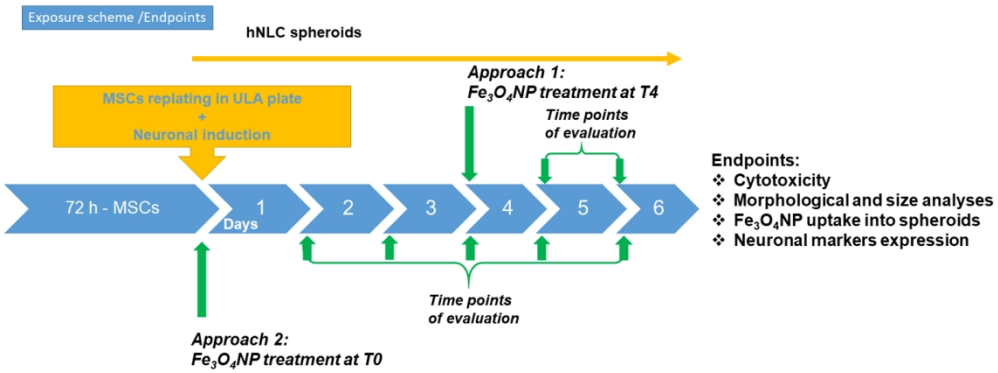

Fig. 1. Exposure approach. Schematic overview depicting the design of the two Fe_3O_4NP exposure approaches and endpoints applied in this study. In the first approach the hNLC spheroids were treated with increasing concentrations of Fe_3O_4NPs at day 4 (T4) of the neurogenic induction; in the second approach, hNLCs were treated with Fe_3O_4NPs at time T0 of both spheroid formation and neurogenic differentiation.

135x51mm (300 x 300 DPI)

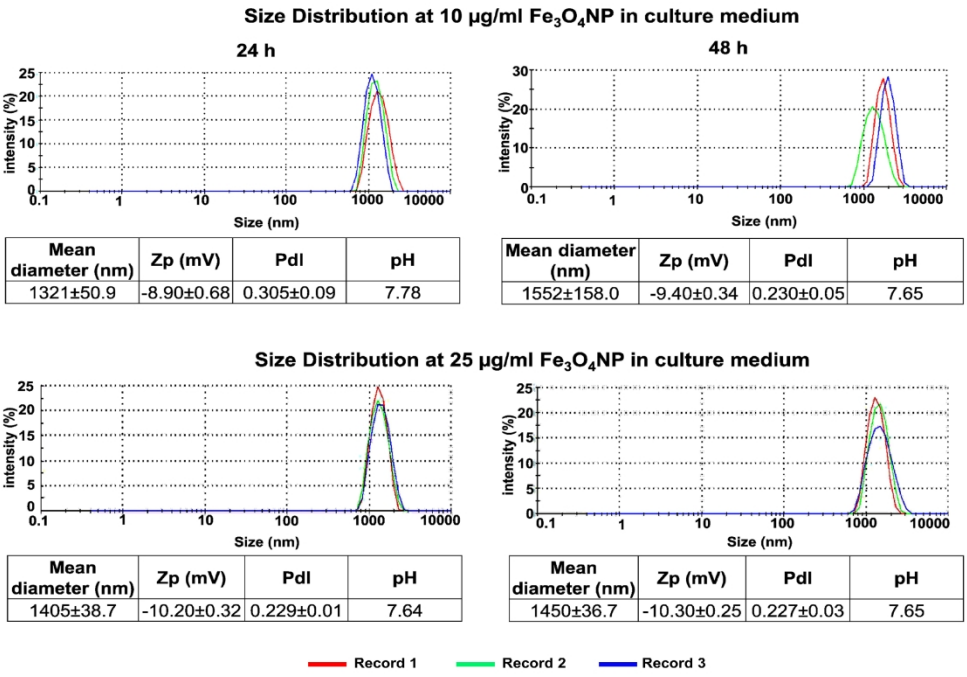

Mean diameter (nm)	Zp (mV)	PdI	pH
1321±50.9	-8.90±0.68	0.305±0.09	7.78

Mean diameter (nm)	Zp (mV)	PdI	pH
1552±158.0	-9.40±0.34	0.230±0.05	7.65

Mean diameter (nm)	Zp (mV)	PdI	pH
1405±38.7	-10.20±0.32	0.229±0.01	7.64

Mean diameter (nm)	Zp (mV)	PdI	pH
1450±36.7	-10.30±0.25	0.227±0.03	7.65

Fig. 2. Physico-chemical properties of the Fe_3O_4NPs in culture medium. Size distribution of the Fe_3O_4NP suspensions at 10 and 25 µg/ml in neurogenic medium after 24 and 48 h evaluated by dynamic light scattering. The tables summarize the physico-chemical properties of the Fe_3O_4NP suspension. Zp, zeta potential; PdI, polydispersity index.

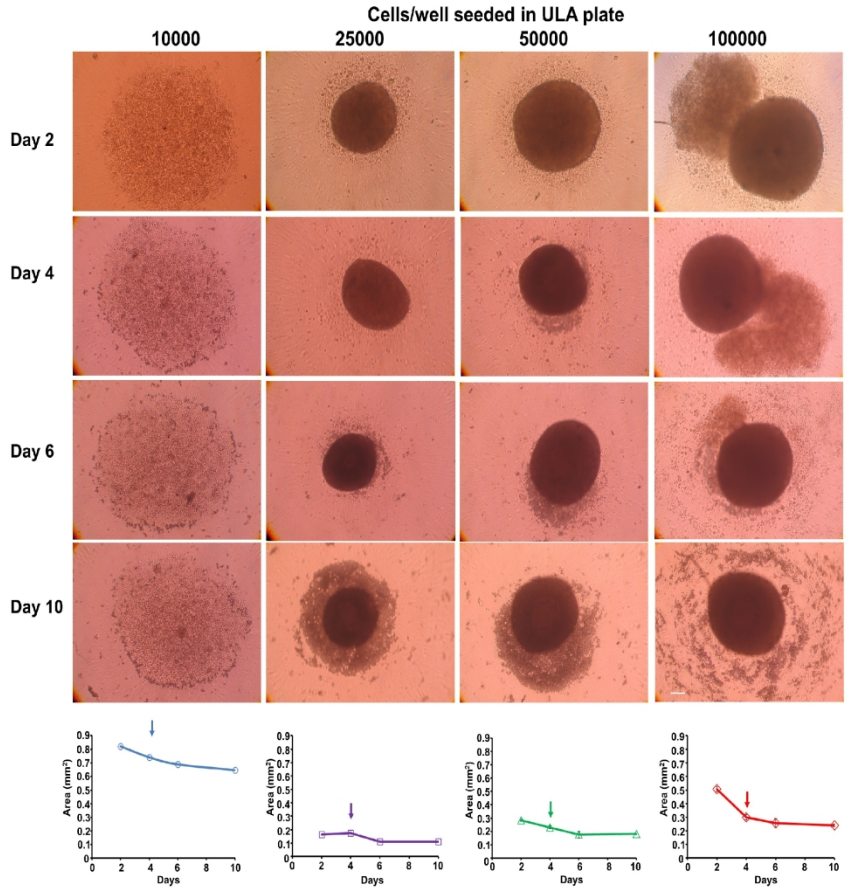

Days	Cells/well seeded in ULA plate			
	10000	25000	50000	100000
2	Loose aggregate immediatelly	Compact	Compact	Compact, together with loose cells on periphery
4		Tight aggregate	Compact, together with loose cells on periphery	Loss of compactness, cells dispersed peripherally
6		Compact, together with loose cells on periphery	Loss of compactness, together with loose cells on periphery	Loss of compactness, increase of cells dispersed peripherally
10		Loss of compactness, together with loose cells on periphery	Loss of compactness, increase of cells dispersed peripherally	

Fig. 3. Characterization of hNLC spheroids over time at different cell numbers seeded. Representative images of hNLCs spheroids in 96 ULA plate seeded at the cell density indicated in the figure during time (from day 2 to day 10). The graphic/plot shows the size (area) of hNLC spheroids at different cell density for each time point considered. Table summarizes the morphological changes observed over time for each cell density.

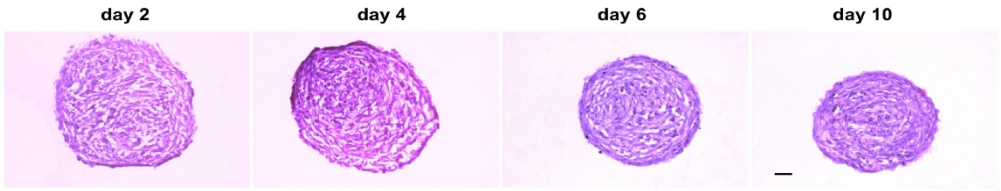

Diameter (µm)			
458 ± 1.8	473 ±2.7	376 ± 2.3	375 ± 1.9

Fig. 4. hNLC spheroid sections over time after H&E staining. No difference in morphology was observed during time: hNLC spheroids showed a well-defined circular structure. The cells on the outside were elongated compared to those on the inside formed by triangular-shaped cells with a round nucleus. Necrotic core or hypoxia, in term of reduced cell density, apoptotic nuclei and lighter eosin staining, was not evidenced. No necrotic core or hypoxia was present. The cells were seeded at 25000 cells/well, and hNLC spheroids were cultured up to 10 days. It has been advocated the use of at least 18-24 replicates per condition as spheroids can be lost during feeding or transfer. Diameter was expressed as mean ± S.E. Scale Bar 50 µm.

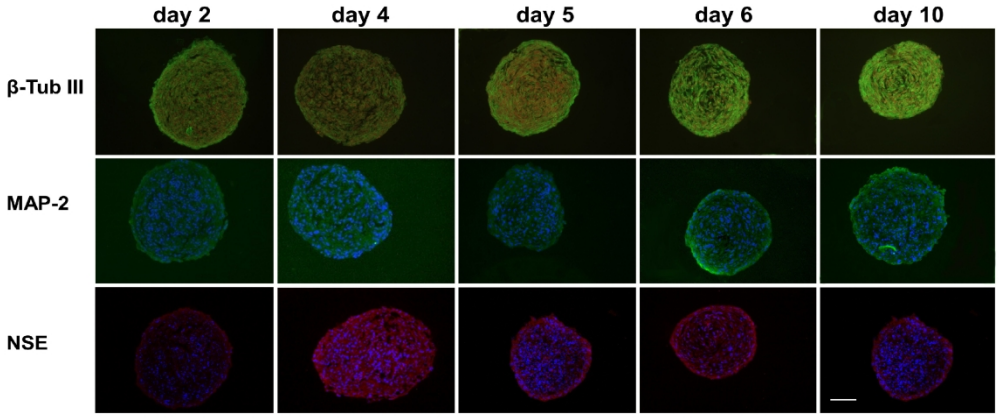

Fig. 5. Immunofluorescence analysis of the neuronal marker expression in hNLC spheroids. Representative fluorescence merged images of hNLC spheroid sections labelled for β-Tub III (structural marker, green), MAP-2 (mature neuron marker, green) and NSE (cytoplasmic protein expressed by mature neuron, red). The fluorescence pattern of each neuronal marker in hNLC spheroids cultured in neurogenic medium increased from day 2 to day 10. Nuclei were counterstained with Hoechst 33258. Scale bar: 100 μm.

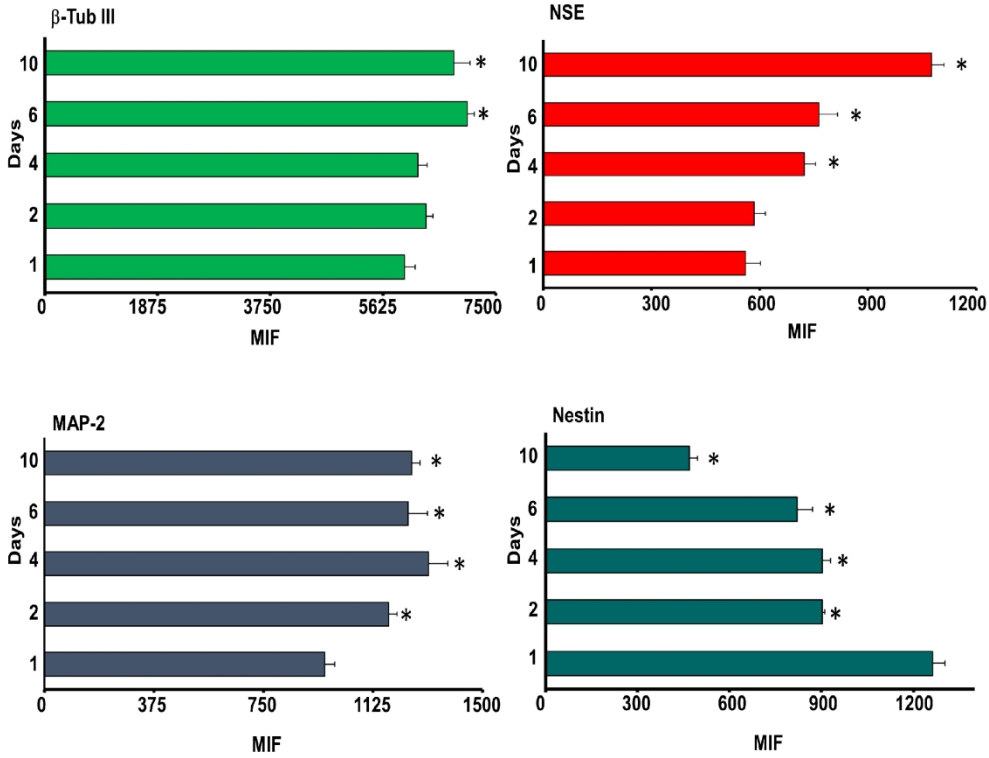

Fig. 6. Flow cytometry analysis of the neuronal marker expression in hNLC spheroids. Neuronal marker expression (β-Tub III, MAP-2, NSE, Nestin) was evaluated during time from day 1 to day 10. Data are expressed as MFI and represent the mean ± S.E. * $p < 0.05$, statistical analysis by ono-way ANOVA followed by Tukey's multiple comparisons test.

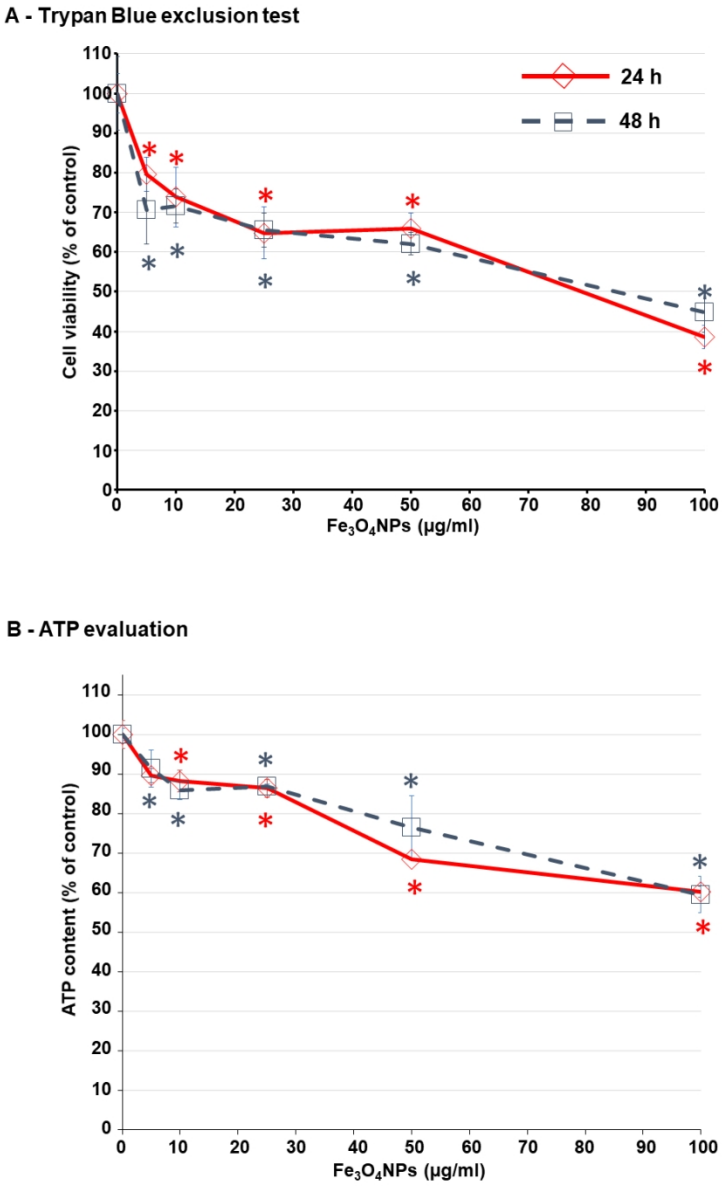

Fig. 7. Cytotoxicity effects after Fe_3O_4NPs exposure in hNLC spheroids treated at T4. Cell viability evaluation by Trypan blue (TB) exclusion test (A) and ATP content evaluation (B) in hNLC spheroids treated with increasing concentration of Fe_3O_4NPs (5-100 µg/ml) for 24 and 48 h exposure. Data are normalized to the mean value obtained under control condition and expressed as percentage (% of each control) and plotted as the mean ± S.E. * $p < 0.05$, statistical analysis by one-way ANOVA followed by Tukey's multiple comparisons test.

81x131mm (300 x 300 DPI)

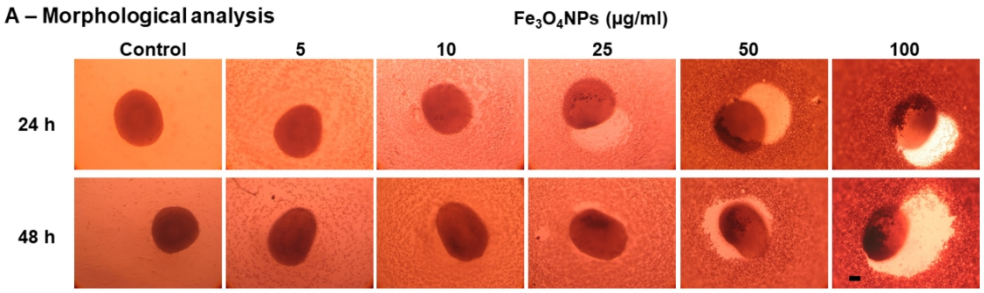

B – Spheroid area

Fe_3O_4NPs (µg/ml)

Time (h)	Control	5	10	25	50	100
24	100±0.8	96.7±2.4	97.6±1.0	94.4±0.7*	91.9±1.1*	89.3±2.0*
48	100±1.4	99.5±1.6	98.7±1.0	90.2±0.7*	89.6±1.3*	87.4±0.9*

Fig. 8. hNLC spheroid growth treated at T4. Morphological analysis (A) and spheroid area estimation (B) of the hNLC spheroids treated at T4 and evaluated after 24 and 48 h exposure to increasing Fe_3O_4NP concentrations (5-100 µg/ml). No morphological alteration was observed after Fe_3O_4NP exposure. The calculated area revealed that Fe_3O_4NP treatments resulted in reduction starting from 25 µg/ml already after 24 h without exacerbation after 48 h. hNLC spheroid area was calculated by Image J software. Data are normalized to the mean value obtained under control condition (area of control at 24 h: 0.171 ± 0.004 mm^2; area of control at 48 h: 0.163 ± 0.007 mm^2) and expressed as mean ± S.E. Scale Bar: 100 µm.

108x56mm (300 x 300 DPI)

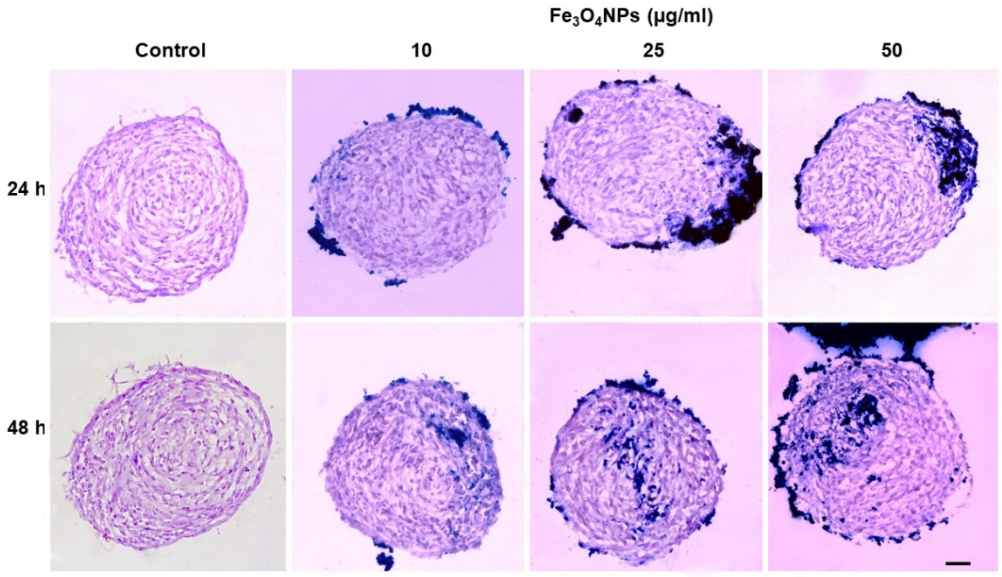

Fig. 9. Fe_3O_4NP uptake in hNLCs treated at T4. Qualitative evaluation of Fe3O4NPs uptake using Perls' Prussian blue staining in hNLC spheroids treated with increasing concentration of Fe_3O_4NPs (10-50 µg/ml) at T4 for 24 and 48 h exposure. Fe_3O_4NP uptake into hNLC spheroids was concentration- and time-dependent as showed in representative micrographs of hNLC spheroid sections. Fe_3O_4NPs, at the lowest concentration tested, were visible on the surface and in the outer layers of the spheroid; at the higher Fe_3O_4NP concentrations (25-50 µg/ml) and continuing with the exposure (48 h), Fe_3O_4NPs were observed in the inner layers of spheroids reaching also the core of hNLC spheroids. Scale Bar: 50 µm

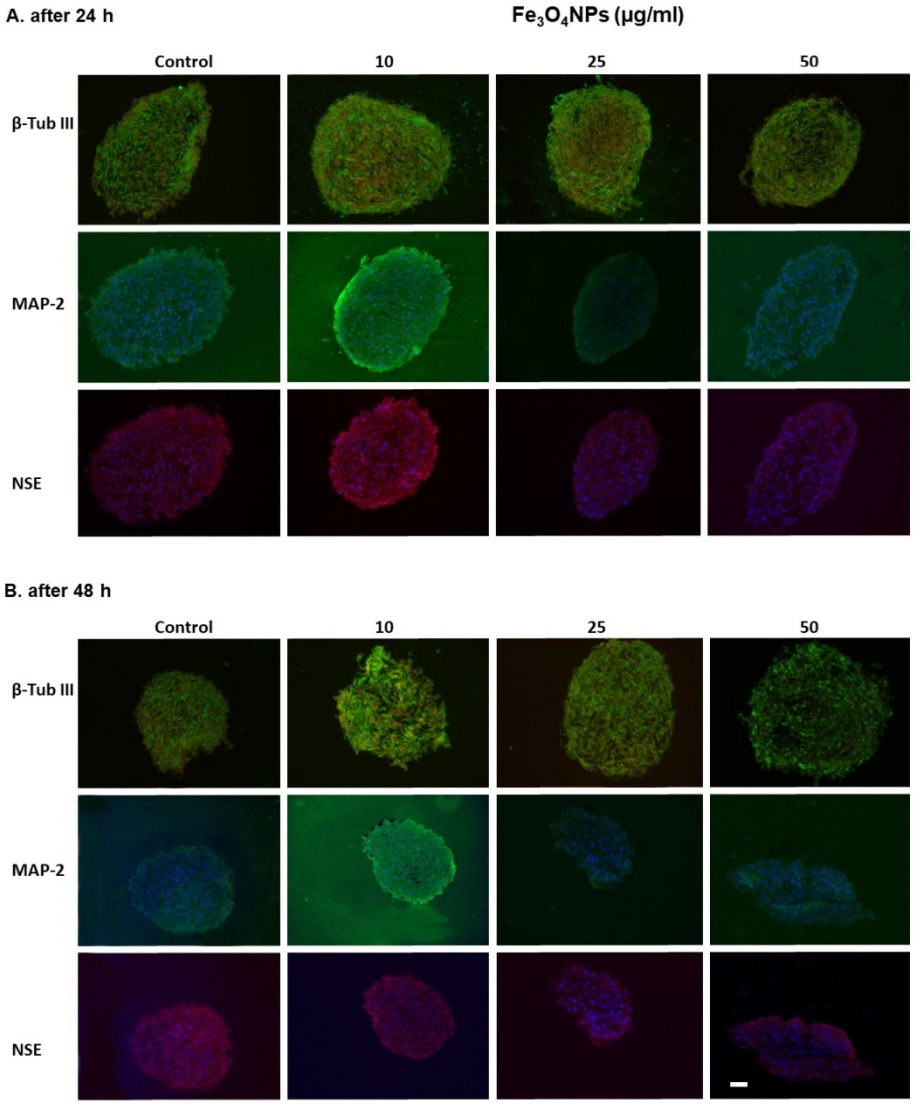

Fig. 10. Immunofluorescence analysis of neuronal markers in hNLCs treated at T4. Representative fluorescence merged images of hNLC spheroid sections after 24 (A) and 48 h (B) exposure with increasing concentration of Fe_3O_4NPs (10-50 µg/ml). A reduction of the MAP-2 and NSE fluorescence pattern at 50 µg/ml and 25 µg/ml respectively was visible after 24 h exposure and for both at 25 µg/ml after 48 h. While, a decrease β-Tub III fluorescence was observed after 48 h only. Scale Bar: 100 µm.

108x121mm (300 x 300 DPI)

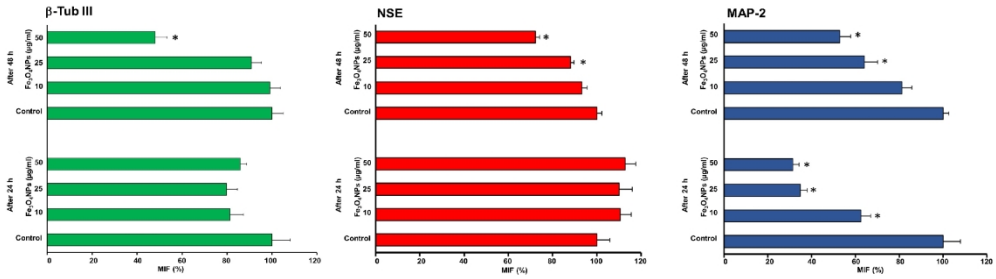

Fig. 11. Flow cytometry analysis of the neuronal marker expression in hNLC spheroids treated at T4. Neuronal marker expression (β-Tub III, NSE, MAP-2) was evaluated after 24 and 48 h exposure to increasing concentration of Fe_3O_4NPs (10-50 μg/ml). Data are expressed as MFI percentage (% of respective control) and plotted as the mean ± S.E. * $p < 0.05$, statistical analysis by ono-way ANOVA followed by Tukey's multiple comparisons test.

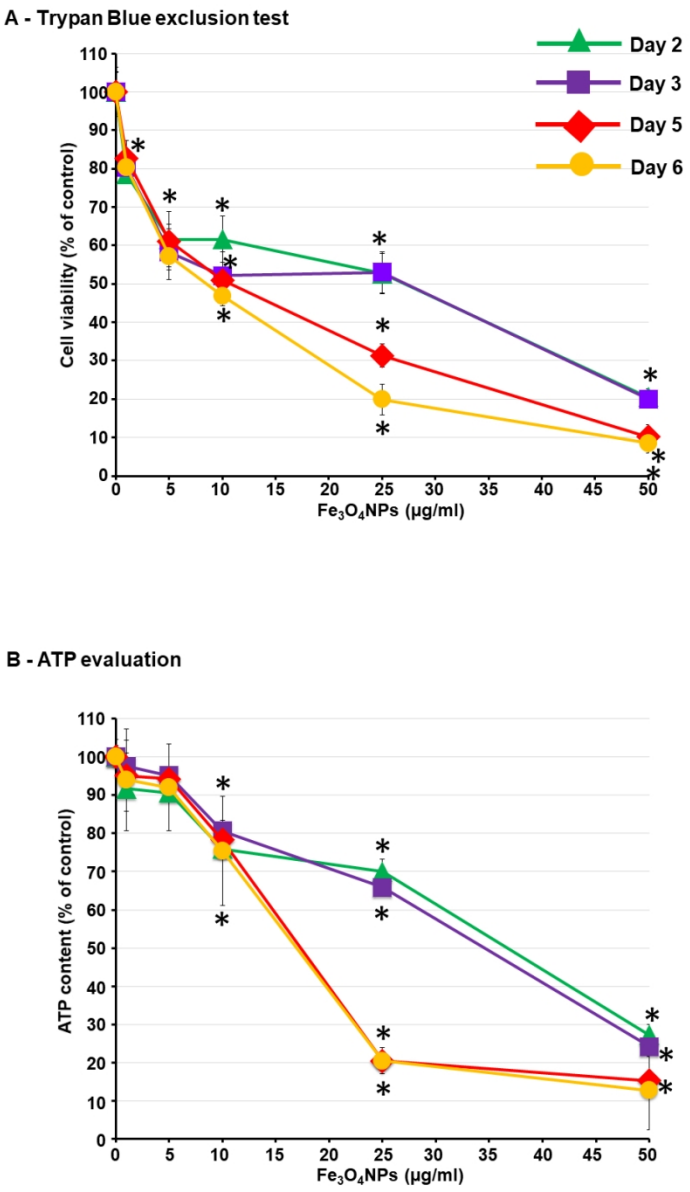

Fig. 12 Cytotoxicity effects after Fe_3O_4NPs exposure in hNLC spheroids treated at T0. Cell viability evaluation by Trypan blue (TB) exclusion test (A) and ATP content evaluation (B) in hNLC spheroids treated with increasing concentration of Fe_3O4NPs (1-50 µg/ml) at T0. The assessments were performed at day 2, 3, 5, 6. Data are normalized to the mean value obtained under control conditions and expressed as percentage (% of each control) and plotted as the mean ± S.E. * $p < 0.05$, statistical analysis by one-way ANOVA followed by Tukey's multiple comparisons test.

81x135mm (300 x 300 DPI)

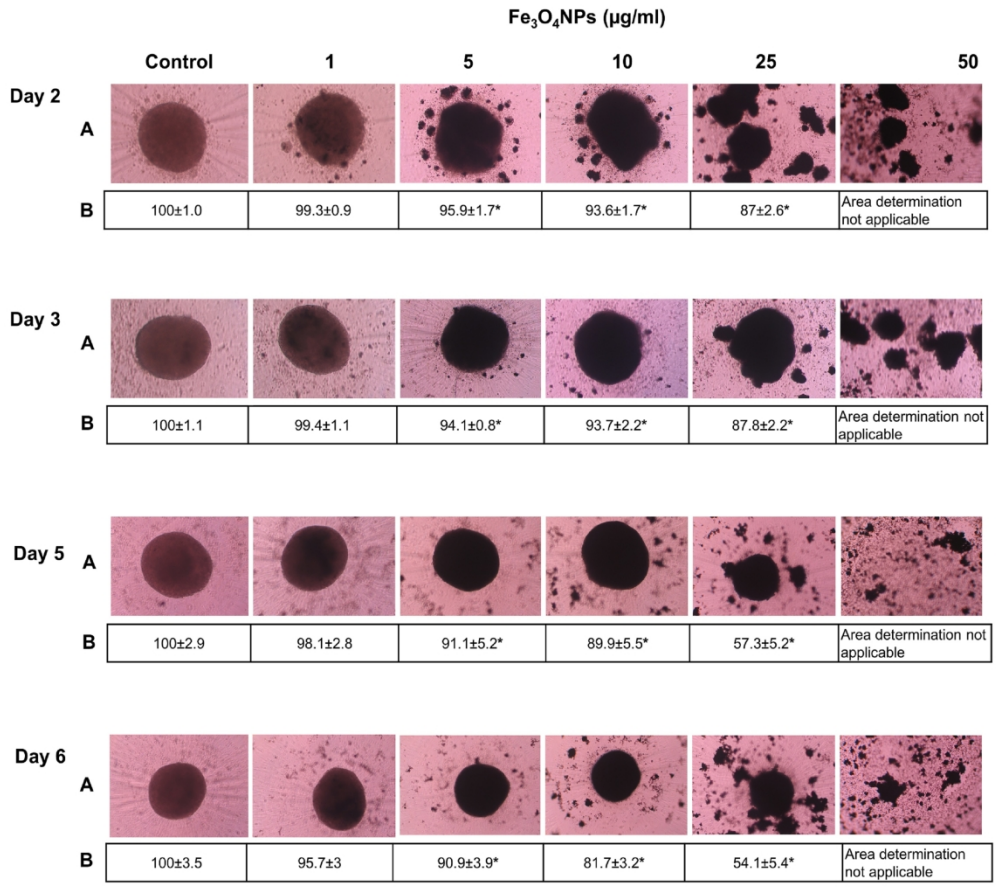

Fig. 13. hNLC spheroid growth treated at T0. Morphological analysis (A) and spheroid area estimation (B) of the hNLC spheroids treated at T0 with increasing Fe_3O_4NP concentrations (1-50 µg/ml). hNLC spheroids displayed loss of compactness, together with loose cells on periphery associated with an area reduction starting from 5 µg/ml already at day 2 with exacerbation at higher concentrations and persisting up to day 6.

hNLC spheroid area was calculated by Image J software. Data were normalized to the mean value obtained under control conditions (area of control at day 2: 0.165 ± 0.0003 mm^2; area of control at day 3: 0.169 ± 0.002 mm^2; area of control at day 5: 0.170 ± 0.001 mm^2; area of control at day 6: 0.124 ± 0.001 mm^2) and expressed as mean ± S.E. Scale Bar 100 µm.

245x220mm (300 x 300 DPI)

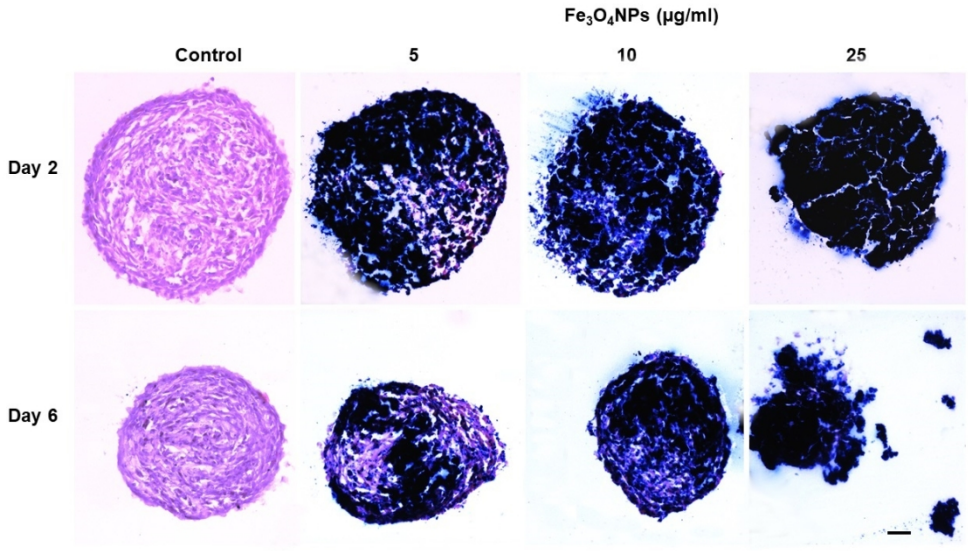

Fig. 14. Fe_3O_4NP uptake after T0 treatment. Qualitative evaluation of Fe_3O_4NPs uptake using Perls' Prussian blue staining in hNLC spheroids treated with increasing concentration of Fe_3O_4NPs (5-25 µg/ml) at T0. The representative images of hNLC spheroid sections indicated that Fe3O4NPs were immediately detectable in the core of hNLC spheroids already at day 2. An overload of NPs was observed already at the lowest concentration tested (5 µg/ml), increased at the higher concentrations (10-25 µg/ml), and persisted up to day 6. Scale Bar 50 µm.

108x60mm (300 x 300 DPI)

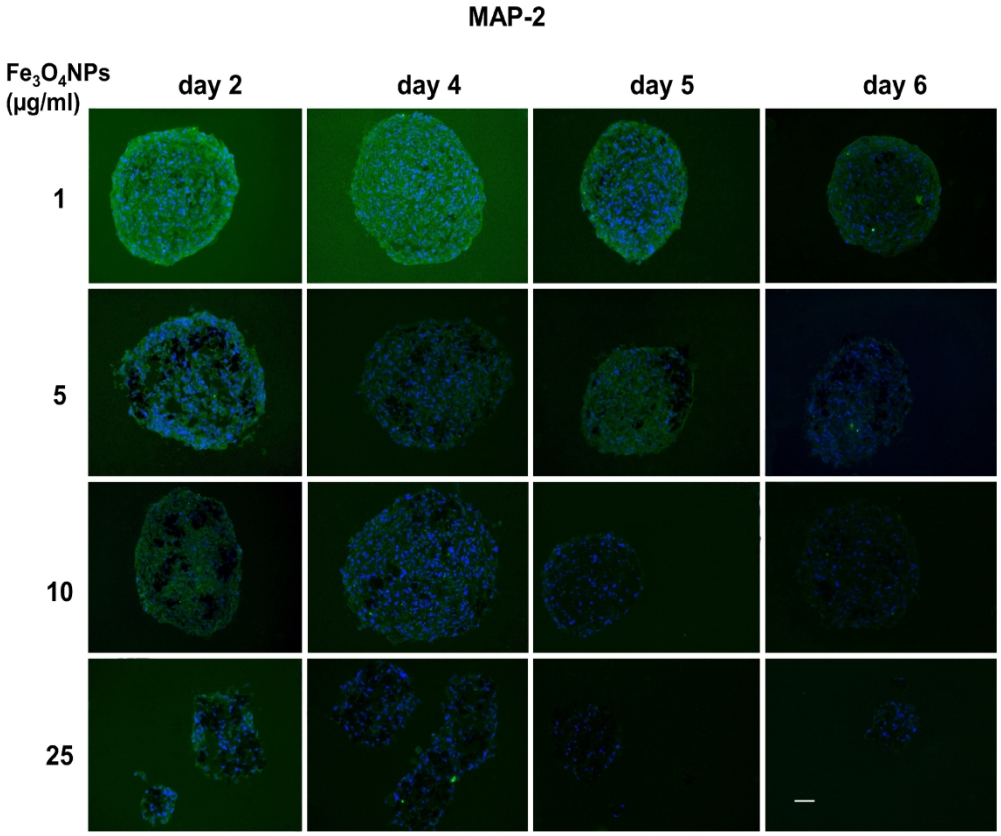

Fig. 15. Immunofluorescence analysis of MAP-2 in hNLCs treated at T0. Representative fluorescence merged microphotographs of hNLC spheroid sections showing the Fe_3O_4NP effects on MAP-2 (Microtubule-associated protein 2). The fluorescence decrease started from 10 µg/ml already at day 2 with exacerbation during time. Nuclei were counterstained with Hoechst 33258. Scale Bar: 100 µm.

295x248mm (300 x 300 DPI)

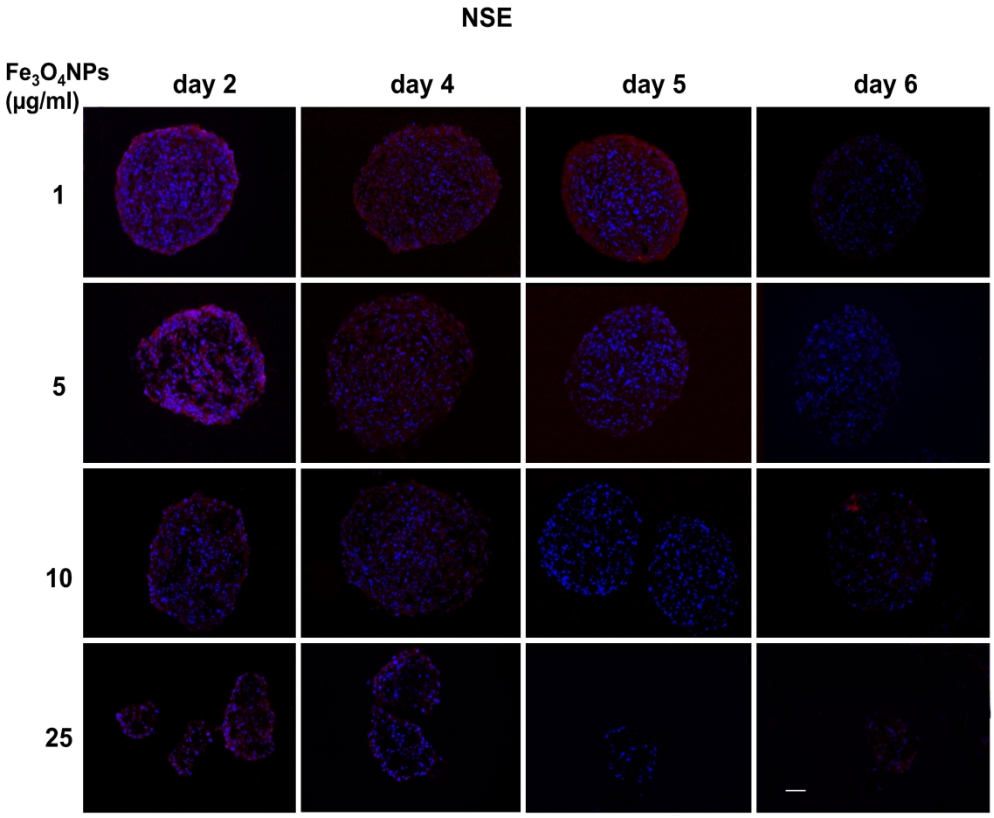

Fig. 16. Immunofluorescence analysis of NSE in hNLCs treated at T0. Representative fluorescence merged microphotographs of hNLC spheroid sections showing the Fe_3O_4NP effects on NSE (enolase) expression. The fluorescence decrease started from 10 µg/ml already at day 2 with a strong exacerbation at lowest concentration (≥ 1 µg/ml) tested at day 5 and day 6. Nuclei were counterstained with Hoechst 33258. Scale Bar: 100 µm.

299x245mm (300 x 300 DPI)

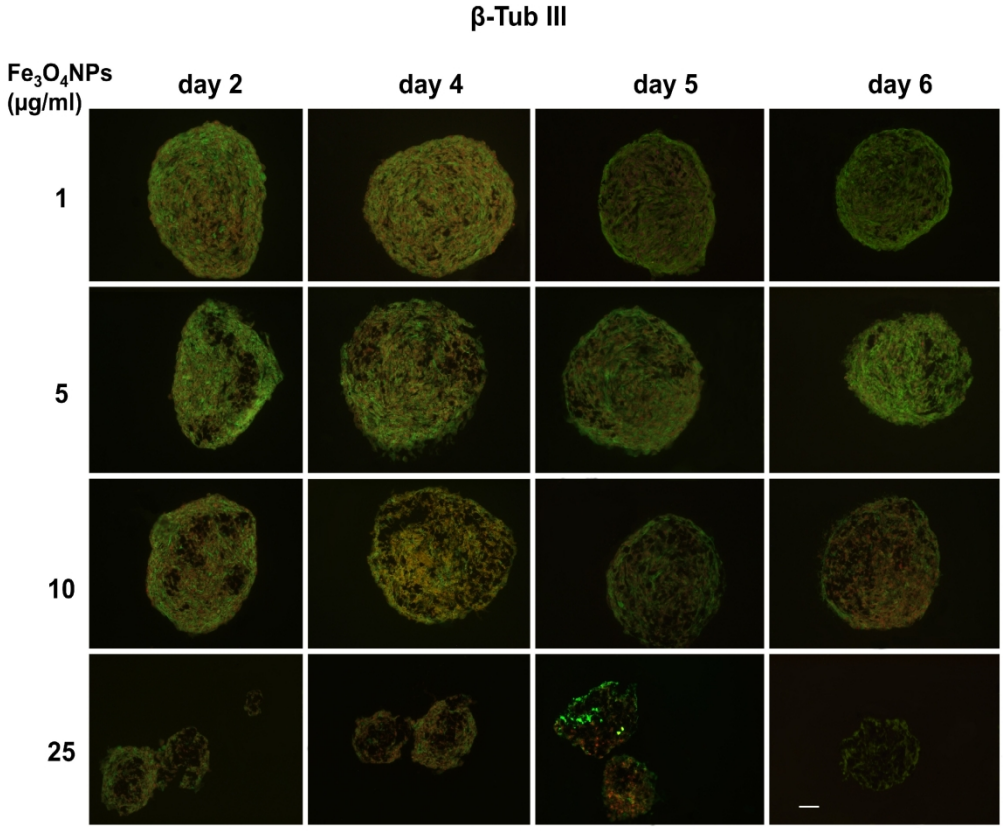

Fig. 17. Immunofluorescence analysis of β-Tub III in hNLCs treated at T0. Representative fluorescence merged microphotographs of hNLC spheroid sections showing the Fe_3O_4NP effects on β-Tub III. A reduction of fluorescence was observed from day 4 at the highest concentration tested (25 μg/ml) with exacerbation at day 5 and day 6. Nuclei were counterstained with Hoechst 33258. Scale Bar: 100 μm.

295x247mm (300 x 300 DPI)

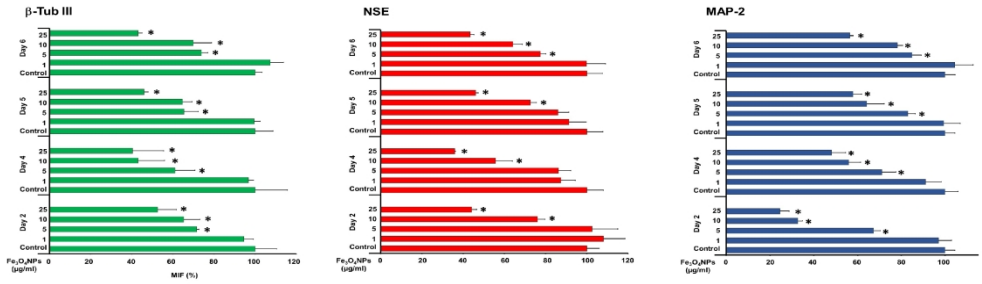

Fig. 18. Flow cytometry analysis of the neuronal marker expression in hNLC spheroids treated at T0. Neuronal marker expression (β-Tub III, NSE, MAP-2) in hNLC spheroids treated with increasing concentration of Fe_3O_4NPs (1-25 μg/ml) was evaluated at T0 and at different time points. Data are expressed as MFI percentage (% of respective control) and plotted as the mean ± S.E. * $p < 0.05$, statistical analysis by ono-way ANOVA followed by Tukey's multiple comparisons test.

Figure S1: Control trend over time from 2 to 6 days. Control value of viable cell number and spheroid area (A), and ATP content (B) as a function of time. Data are plotted as the mean ± S.E.